catalysts

MDPI

Review

Ultradurable Pt-Based Catalysts for Oxygen Reduction Electrocatalysis

Ziting Li [1], Peng Zhou [1], Yuxin Zhao [1], Wenyue Jiang [1], Bingxin Zhao [1], Xiaoshuang Chen [1,2,*] and Menggang Li [3,*]

[1] College of Chemistry and Chemical Engineering, Qiqihar University, Qiqihar 161006, China
[2] Heilongjiang Provincial Key Laboratory of Surface Active Agent and Auxiliary, Qiqihar University, Qiqihar 161006, China
[3] School of Materials Science & Engineering, Peking University, Beijing 100871, China
* Correspondence: cxshuang1988@163.com (X.C.); shulmg@163.com (M.L.)

Abstract: An oxygen reduction reaction (ORR) is the key half reaction of proton exchange membrane fuel cells (PEMFCs), and is highly dependent on Pt-based nanocrystals as core electrocatalysts. Despite the exceptional ORR activity from adjusting the electronic structures of surface or near-surface atoms, several serious issues, including the corrosion of carbon supports, the preferential leaching of active metal elements, the instability of surface low-coordinated atoms and the sintering/agglomeration of nanocrystals, still exist, challenging the ORR durability of developed Pt-based ORR catalysts. From the point of view of the catalyst structure design, in this review, we summarized the state-of-the-art structural regulation strategies for improving the ORR durability of Pt-based catalysts. The current limitation of Pt-based binary catalysts for ORR electrocatalysis is firstly discussed, and the detailed strategies are further classified into the optimization of supports, metal-doped alloys, core/shell structures, intermetallics and high-entropy alloys, etc. The structure–performance relationship is detailedly explained, especially emphasizing the elimination of the above restrictions. Finally, the existing challenges and future research direction are further presented, aiming at practicing the PEMFC devices of the ultradurable Pt-based catalysts.

Keywords: platinum; alloys; oxygen reduction reaction; durability; fuel cells

Citation: Li, Z.; Zhou, P.; Zhao, Y.; Jiang, W.; Zhao, B.; Chen, X.; Li, M. Ultradurable Pt-Based Catalysts for Oxygen Reduction Electrocatalysis. *Catalysts* **2024**, *14*, 57. https://doi.org/10.3390/catal14010057

Academic Editor: Carlo Santoro

Received: 12 November 2023
Revised: 9 January 2024
Accepted: 10 January 2024
Published: 12 January 2024

1. Introduction

The ever-increasing energy consumption and accelerating environmental destruction have stimulated the development of alternative renewable energy [1–3]. As a favorable candidate for fossil fuels, hydrogen (H_2) has attracted more and more attention due to its high energy density and the absolute cleanliness of its oxidation products, especially the green hydrogen obtained using water electrolysis technology [4–7]. Proton exchange membrane fuel cells (PEMFCs) are the typical devices used to realize the sustainable energy conversion, which have shown the advantages of efficient power generation, low operation temperature and environmental friendliness [8–11]. At the anode, a half reaction of PEMFCs is the hydrogen oxidation reaction (HOR), which generally shows fast kinetics in an acidic medium [12–14]. However, the oxygen reduction reaction (ORR), another key half reaction of PEMFCs, shows extremely slow catalytic kinetics, making the overall efficiency of PEMFCs significantly low [15–21]. Therefore, highly efficient ORR catalysts are necessary, which brings opportunities for state-of-the-art Pt-based materials. Despite the extensive applications, the low CO tolerance, poor durability and high cost of Pt catalysts limit the further development and application of PEMFCs [22–25]. Although tremendous efforts for seeking efficient and practical ORR electrocatalysts from earth-abundant materials, such as carbon-based and transition metal-based catalysts, their activities are still uncompetitive compared with Pt-based materials [26–29].

A mainstream means for reducing the cost of Pt-based catalysts and improving the ORR catalytic performance is to alloy Pt with nonprecious metals (M) to form PtM alloys or M/Pt core/shell structures [30–33]. The consistency of experiments and theories has proved that alloying can not only improve the utilization efficiency of Pt, but also optimize the adsorption strength towards oxygen-containing intermediates through a potential ligand/strain effect [34–36]. In this case, Hyundai and Toyota have deployed Pt-based alloy nanoparticles for their commercialized fuel cell vehicles rather than pure Pt metals [37,38]. On the other hand, to further increase the exposure of surface-active atoms, a series of anisotropic Pt-based catalysts were developed, such as nanowires, nanotubes, nanoplates, nanoflowers and nanoframes, etc. [39–45]. These unique structures also endow them with stronger interactions between catalysts and supports than their 0D counterparts, thus accelerating the transfer of electrons and protons [46–49]. In addition, the combination of several typical strategies, including defect engineering, (near)-surface regulation and local coordination optimization, etc., can stimulate catalytic activity by adjusting the adsorption of intermediates and enhancing the utilization of active sites [50–54]. These advanced attempts make it possible for various highly active Pt-based ORR electrocatalysts.

Although extraordinary activities have been achieved, the above-mentioned promising results of those Pt catalysts are frequently not reproduced under practical PEMFCs in industry [22,55–58]. This further challenges the durability of these Pt-based catalysts, which is also an important parameter for evaluating their catalytic performance. Considering the aspect of catalysts, the dominant factor for which the stability of catalysts is not enough to meet the actual PEMFCs is the inevitable leaching of nonprecious metals during the operation of the electrocatalytic reactions [59,60]. This is mainly due to the fact that the alloying metals are inherently less resistant than Pt under acidic and oxidative conditions. Moreover, the instability of the exposed active facets with high surface energies is another issue, in that the Pt-based catalysts with an anisotropic morphology cannot operate under a harsh PEMFC environment for a long time [61–63]. This is also the reason why the commercial PEMFC catalysts are alloy nanoparticles instead of having highly controlled morphologies [9,64]. The utilization of carbon supports is also a bottleneck to improve the stability of PEMFCs, because carbon supports will be seriously oxidized and corroded during the electrochemical process, especially under transient conditions such as startup or shutdown as well as the local fuel starvation events at the anode [55,65,66]. This will lead to the separation and aggregation of Pt particles, decreasing the electrochemical specific areas (ECSAs). Over the past several decades, tremendous progress has been made in developing highly durable Pt-based ORR catalysts and exploring their degradation mechanisms [10,67–71]. Therefore, a report which can systematically review the strategies to boost the durability of Pt-based ORR catalysts and establish the degradation mechanism from the atomic scale seems timely and significant.

In this review, several typical strategies to alleviate the degradation and improve the durability of Pt-based alloys during ORR electrocatalysis will be systematically summarized. The mechanism of the PEMFC operation and the essential reasons behind the degradation of Pt-based catalysts will be firstly elucidated. Then, a series of latest strategies for designing ultradurable Pt-based catalyst systems will be proposed, mainly including the optimization of supports, metal-doped alloys, core/shell structures, intermetallics and high-entropy alloys, etc. (Scheme 1). The improved mechanism behind these advanced systems will be focused on the structure–property relationship. These ultradurable Pt-based catalysts are anticipated to show promising applications in ORR electrocatalysis. Finally, this hot field is prospected from the aspects of catalysts and support structure designs, the structure–activity relationship revealed through in situ characterizations and the integration of multiple advantages, with the purpose of promoting the fruitful research in the field of PEMFCs.

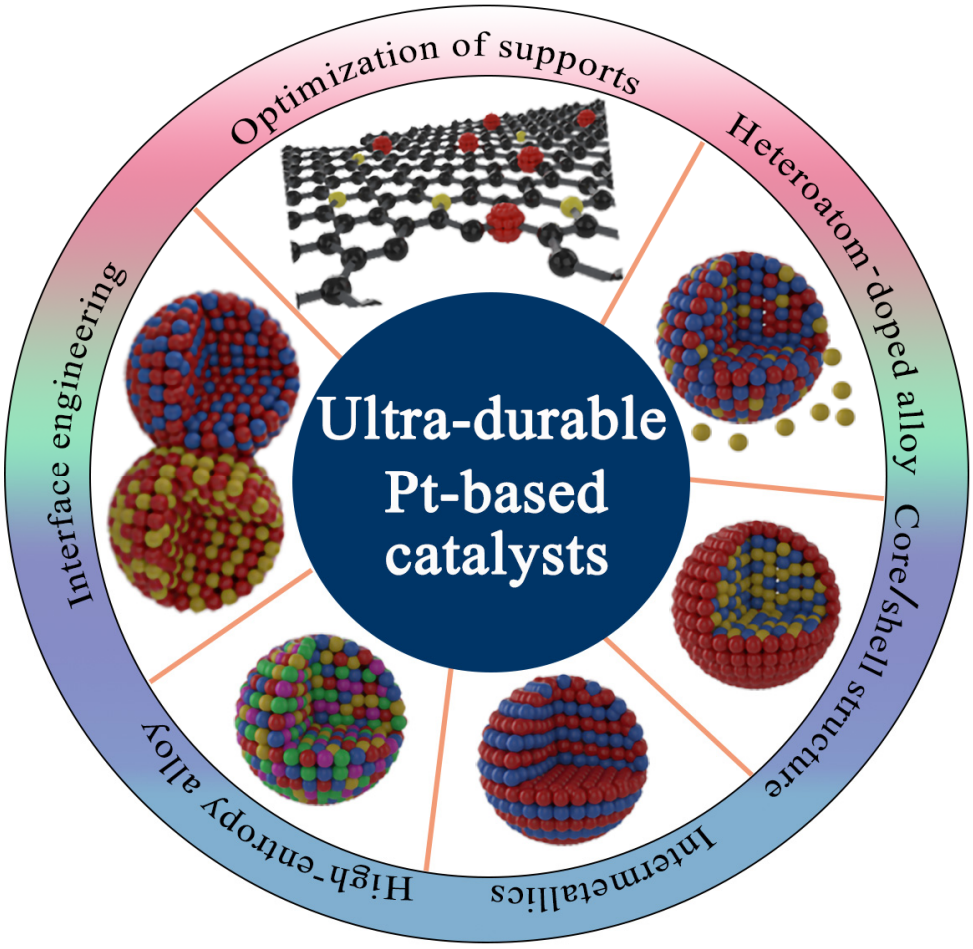

Scheme 1. Typical strategies for enhancing ORR durability of Pt-based catalysts.

2. Operation Mechanism of ORR Electrocatalysis

In the cathode of PEMFCs, O_2 is electrochemically reduced through ORR electrocatalysis, mainly involving either the direct four-electron reduction pathway from O_2 to H_2O or the two-electron reduction pathway from O_2 to H_2O_2. Generally, the favorable path for PEMFCs is the direct four-electron reduction pathway, because H_2O_2 will accelerate the degradation of the proton-conducting polymer electrolyte and reduce the energy-conversion efficiency. The oxygenated (O*), hydroxyl (OH*) and superhydroxyl (OOH*) species are several dominant intermediates for ORR electrocatalysis, of which mutual transformations complicate the ORR process (Figure 1a) [72]. To date, there is still no accurate explanation to determine the ORR rate-determining step. As a matter of fact, three possible rate-determining steps have been proposed, involving the first electron transfer to an adsorbed O_2 molecule, the hydration of O_2 and the final desorption of H_2O [73]. However, the underlying mechanism is still under debate, which is mainly due to the complex reaction pathway depending on the catalyst type and operation environment, including the solvent, temperature and applied potential. In addition, oxygen coverage may affect the ORR performance, supported by associative and dissociation mechanisms. Specifically, a high oxygen coverage induces the O–O cleavage after the formation of OOH*, while the low one cleaves the O–O bond before the formation of OH* [74,75].

According to the adsorbed O_2 dissociation mechanism, the ORR activity can be depicted as a function of O* or OH* binding energy. To clearly elucidate the rule of binding energy towards ORR intermediates on various metals, a well-known "volcano"-type plot was depicted (Figure 1b) [76]. Under the guidance of this rule, the metals (such as Au) with a more positive binding energy than Pt show a lower ability for adsorbing O* or OH*; thus, the transfer of protons and electrons to oxygen cannot occur. However, the

metals (such as Ni) with a more negative binding energy than Pt tend to bind O* or OH* strongly to induce the very slow step for transferring protons. By comparison, Pt possesses the optimal binding energy towards O* and OH*, thereby becoming a best ORR catalyst located at the apex of the volcano curve. Alloying Pt with other metals can further optimize the ORR performance. Similarly, the volcano trend can be found in terms of the *d*-band center for these Pt-based alloy catalysts (Figure 1c) [77]. In this case, two opposing effects, the strong adsorption energy of O_2 and intermediates and the low coverage by adsorbed anions, can also be observed on the Pt-based alloys, which are highly similar to those of single metal catalysts. Consequently, the ORR reaction rate is limited by the availability of OH*/anion-free Pt sites due to the strong binding of O_2 molecules on Pt. For example, in the case of Pt_3Ti and Pt_3V, due to the fact that the *d*-band center is too far away from the Fermi level, the surface is less covered by OH* and anions, while the low adsorption energy of O_2 is found, thus limiting the ORR electrocatalysis.

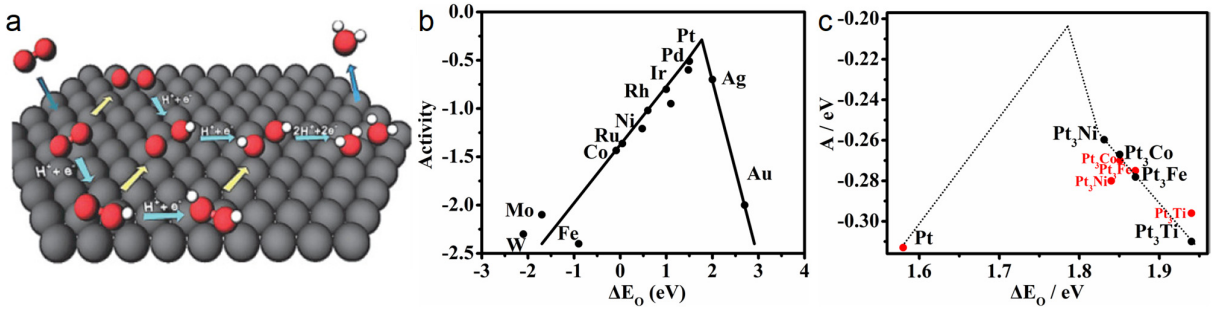

Figure 1. Reaction mechanism of ORR electrocatalysis. (**a**) Illustration scheme of various possible ORR intermediates and mechanisms. (The gray, red and white spheres represent catalyst, oxygen and hydrogen atoms, respectively. The yellow and blue arrows display O–O bond cleavage step and the proton or electron transfer process). Reprinted with permission from Ref. [72]. Copyright 2016 Wiley. Relationships between ORR activity of (**b**) different metals and (**c**) Pt_3M alloys vs. the oxygen binding energy. Reprinted with permission from Refs. [76,77]. Copyright 2004 ACS; copyright 2006 Wiley.

3. Limitation of Traditional Pt-Based ORR Catalysts

Although exceptional activity of Pt-based catalysts has been achieved, only a few Pt-based catalysts are used in practical PEMFCs due to the limitation of durability. This is because of the fact that most Pt-based alloys tend to experience obvious structural and compositional evolutions to lose their activity under long-term operation [78,79]. In fact, the degradation of the overall performance is not only related to the catalytic layer, but also closely related to the membrane electrode assembly (MEA) system, such as the ionomer distribution and catalyst–ionomer interface structure, ionomer adsorption on the active surface as well as local oxygen transport resistance [22,80]. However, in this review, we pay more attention to the influence of the catalyst structures on stability, which is because of the fact that the cost of the catalysts occupies the main body of the whole MEA. The first thing to be mentioned is the oxidation of the carbon supports caused by the relatively low CO_2/C standard potential (0.207 V vs. normal hydrogen electrode (NHE)) (Figure 2a). The corrosion of the carbon supports becomes especially obvious when the cathode potential is as high as 1.5 V (vs. NHE) during the event of start/stop or H_2 starvation. Therefore, the porous structure of the carbon supports will collapse, weakening the interaction with the Pt particles and accelerating the shedding and degradation of particle catalysts [81,82].

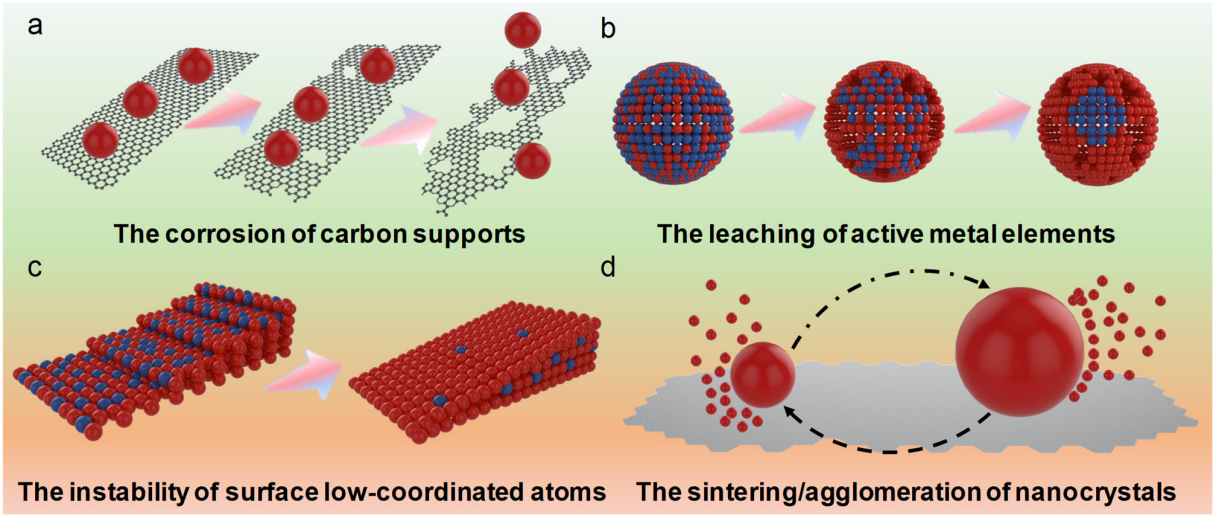

Figure 2. Illustration schemes of dominant limitations of traditional Pt-based catalysts for ORR. (**a**) The corrosion of carbon supports. (**b**) The leaching of active metal elements. (**c**) The instability of surface low-coordinated atoms. (**d**) The sintering/agglomeration of nanocrystals.

Compared with pure Pt, binary or ternary Pt-based alloy catalysts tend to display an enhanced electrocatalytic performance. For example, alloying Ga and Pt atoms can achieve an unconventional p–d hybridization interaction to obtain remarkable ORR activity and durability [39]. In addition to the corrosion of carbon supports, the preferential leaching of active metal elements is also a non-negligible issue (Figure 2b). Generally, Pt has a higher dissolution potential than the alloying metals, including Fe, Co, Ni and Cu, etc. which gives the non-noble metals a greater dissolution tendency [55,57]. Therefore, although the alloying of transition metals is beneficial for enhancing the catalytic activity, their dissolution may lead to the decline in ORR performance. In addition, under acidic conditions, the dissolved metals are more willing to form cations, with a stronger affinity for sulfonic acid groups than protons. They are also undesirable for ORR electrocatalysis.

In half-cell conditions, compared with 0D counterparts, those with an anisotropic morphology often show better ORR performance due to the increased active sites, the enhanced electron and mass transport as well as the improved chemical stability [47,83]. However, most of these anisotropic Pt-based nanocrystals possess the exposed active facets with high surface energy, which are unstable during long-term ORR tests (Figure 2c). Especially for the nanocrystals with high-index facets, the surface low-coordinated atoms will be destroyed during the electrocatalytic processes, despite the fact that they have displayed remarkable catalytic activity [63,84–86]. This is also the dominant reason why most of anisotropic nanocrystals are not suitable for MEAs, thus necessitating further optimization of the surface and/or near-surface atomic structures to boost ORR durability.

The sintering and agglomeration of catalysts are also the main factors affecting the ORR durability of nanocrystals (Figure 2d). Under the long-term operating conditions, the agglomeration of catalysts is inevitable due to the electrochemical Ostwald ripening phenomenon [87–89]. In other words, owing to the excellent electronic conductivity of the carbon supports, the quasiequilibrium is difficult to achieve in the case of two particles with different sizes, leading to the disappearance of small particles and the growth of large particles. Such a sintering process induces the redistribution of Pt sites, decreasing the active sites and attenuating the performance. In order to weaken this undesirable agglomeration phenomenon, the size of the most commonly used catalyst is usually 3–5 nm, while the large size reduces the surface atom utilization of Pt atoms. Nanoparticles with too small of a particle size will aggravate the agglomeration during the catalytic process due to the high surface energy. This also explains why the commercial ORR catalyst are carbon-supported, uniform 3 nm Pt nanoparticles.

4. Main Catalyst Systems for Ultradurable ORR Electrocatalysis

Over the past few decades, superior ORR activity has been observed on numerous Pt-based catalysts, many of which have already exceeded the 2025 DOE target [41,90–92]. However, the main problem is that their structures are difficult to maintain during the potential cycle processes. With the extensive theoretical and experimental research on the Pt surface and the better understanding of the size-dependent trend in ORR electrocatalysis, a series of typical strategies for obtaining highly durable Pt-based catalysts have been developed. Note that the design of these catalysts should not only consider the improvement of durability, but also, the loss of activity cannot be ignored. In this section, we focus on the strategies to improve the durability from the perspective of catalyst structure designs, including the optimization of supports, metal-doped alloys, core/shell structures, intermetallics and high-entropy alloys, etc. The principle of these designs is to solve the problem of durability while maintaining the high activity of the catalysts by optimizing the electronic structure and adsorption energy, such as through inhibiting the loss of transition metals, maintaining the surface-active facets with a high surface energy and improving the anti-agglomeration performance during ORR operations.

4.1. The Optimization of Supports

The utilization of supports is one of the most key factors for affecting the durability of Pt-based catalysts. Generally, enhancing the graphitization can efficiently improve the chemical and thermal stability of carbon supports, presenting several advanced carbon supports including carbon nanofibers, carbon nanotubes, ordered mesoporous carbon spheres and carbon nano-onions, etc. [93–95]. Nevertheless, highly graphitized carbon compromises the specific surface area, porous structure and anchoring sites, challenging the uniform dispersion of Pt-based catalysts, which is unfavorable for the improvement in electrocatalytic activity and durability. To address this issue, it is necessary to introduce functional groups and defect sites through proper surface modifications such as heteroatoms doping, oxidation treatment and polymer modification, aiming at boosting the interaction between the Pt-based nanocrystals and carbon supports [95–98]. In this respect, a 3D N-doped porous graphitic carbon, produced from the carbonization of a 3D polymer hydrogel with the assistance of Mn, was presented as a highly durable and active support to load Pt nanoparticles (Pt/PGC) (Figure 3a) [98]. In this synthesis, the introduction of Mn salts endowed the polymer hydrogel-derived carbon with high graphitization, alleviating the loss of nitrogen doping and the reduction in the surface area caused by the traditional high temperature. Due to the doping of electronegative N atoms, the electronic state of the carbon support was optimized to generate stronger binding between the Pt atoms and bridge sites adjacent to the N dopant compared with the pristine carbon matrix (Figure 3b). Therefore, as-optimized Pt/PGC showed an enhanced ORR electrocatalysis compared with other carbon-supported Pt catalysts, especially in terms of durability. Especially, the advantages of such catalysts in the MEA system are more obvious, reflecting the fact that the voltage loss at a current density of 1.5 A cm^{-2} of the MEA, with Pt/PGC as the cathodic catalyst, is only 9 mV after 5000 potential cycles (Figure 3c). In contrast, the MEA with Pt/TEC10V20E (Vulcan support) showed a more serious attenuation under the similar operation conditions (Figure 3d). In addition to the enhanced durability, the graphitization and porous structure of PGC supports also balance the ORR activity of Pt catalysts.

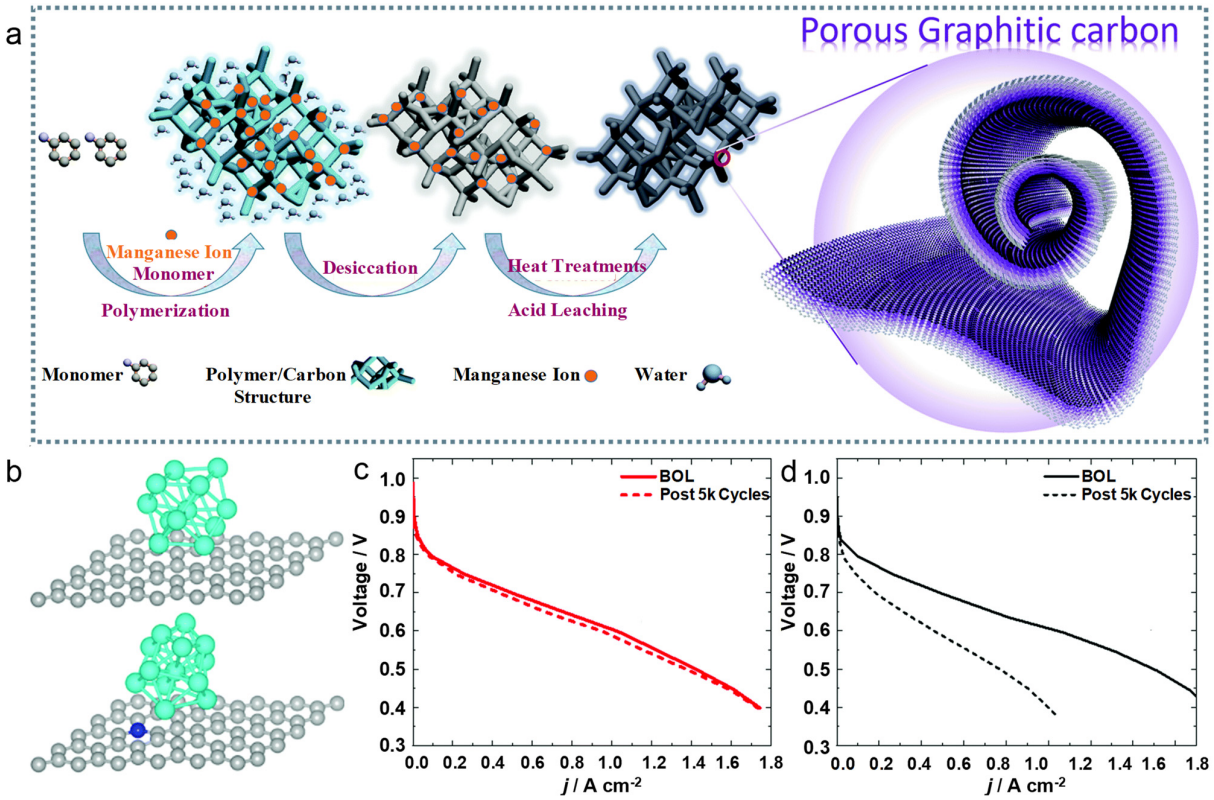

Figure 3. Enhancing ORR durability of Pt−based catalysts by the optimized supports. (**a**) Schematic illustration of the synthesis of PGC derived from a polymer hydrogel. (**b**) Optimized atomic structures of a thirteen-Pt-atom cluster adsorbed on a pristine graphene layer (**top**) and an N-doped graphene layer (**down**) (the gray, cyan and blue balls represent C, Pt and N atoms, respectively). H_2-air fuel cell polarization curves of (**c**) Pt/PGC and (**d**) Pt/TEC10V20E as cathodic catalysts before and after 5000 cycles. Reprinted with permission from Ref. [98]. Copyright 2019 RSC.

Compared with traditional carbon supports, supports embedded with single atoms are more appealing as stable supports to load Pt-based materials. The introduction of single atoms into carbon materials can not only provide a strong interaction between the supports and active metals, but also optimize the adsorption behavior of active Pt-based catalysts, enhancing the ORR performance [99–101]. To this end, Shao's group improved the durability of Pt nanoparticles by using the Fe- and N-codoped carbon (Fe–N–C) [102]. In acidic and alkaline media, the retention rate of ECSAs for the Pt/Fe–N–C catalyst during the potential cycles is much better than that of commercial Pt/C, and the dissolution rate of Pt in Pt/Fe–N–C is three times lower than that of Pt/C. In this catalysis, Fe–N–C supports can provide strong and stable support for Pt nanoparticles, and the formation of oxides can be reduced by adjusting the electronic structure. A strong metal-support interaction and low metal dissolution rate, as well as the highly stable supports are dominant in the remarkable enhancement of Pt/Fe–N–C durability. Therefore, the selection of carbon supports represents a typical strategy for achieving the ultradurable Pt-based catalysis for PEMFCs.

In order to avoid the corrosion of carbon materials, several noncarbon supports with a strong chemical and structural stability have been proposed. For instance, by using mesoporous TiO_2 as the support, Pt/TiO_2 catalysts with a high anticorrosive ability were prepared to enhance the ORR durability [103]. However, metal oxide supports are not a long-term choice due to their poor conductivity and low specific surface area. Therefore, the composites of carbon and metal oxides become potential candidates for promising supports to load Pt-based catalysts to enhance the durability [104]. In the case of metal compound supports, transition metal nitrides and carbides have also been widely spread

around as highly stable support materials, including TiN, WC, CrN and MoN, etc. Very recently, as a kind of emerging 2D transition metal carbide, MXene has been considered as a novel support to load Pt catalysts that can achieve high ORR activity and durability, which is because of the fact that MXene features a unique 2D structure, metallic conductivity, large surface area, abundant surface functional group and high electrochemical stability [105,106].

4.2. Heteroatom-Doped Alloys

Doping engineering is a common strategy for regulating the electronic structures of Pt-based nanocrystals by introducing a small number of foreign atoms into nanocrystals in the form of interstitial or substitution atoms. The doping of heteroatoms can usually inhibit the dissolution of alloying metals, so that alloying metals can play a role in regulating the electronic structure to maintain the activity during the whole test process [107,108]. In addition, this strategy can also maintain the special shape of anisotropic nanocrystals during electrocatalysis [109,110]. More importantly, in terms of the enhanced activity, the doping of heteroatoms can not only adjust the energy band structure to enhance the catalytic activity and selectivity, but also optimize the surface energy of catalysts and control the binding strength towards reaction intermediates to accelerate the reaction kinetics [111–113]. Therefore, doping engineering has been considered as one of the most efficient methods to improve the electrocatalytic performance, not only in terms of durability, but also activity. Moreover, dopants can sometimes participate in the growth of nanocrystals and change the growth mechanism of nanocrystals, inducing the nanocrystals with controllable shapes or phases [114–116].

In light of the fact that the doping of heteroatoms can boost the activity and durability of Pt-based nanocrystals, various transition metals have been introduced into Pt-based alloy catalysts. In this case, a series of transition metals (V, Cr, Mn, Fe, Co, Mo, W and Re) were surface doped into carbon-supported Pt_3Ni octahedra to improve the ORR performance of Pt_3Ni octahedra [117]. Among these well-designed doped catalysts, Mo-doped Pt_3Ni octahedra showed the highest ORR specific activity of 10.3 mA cm^{-2} and a mass activity of 6.98 A $mg_{Pt}{}^{-1}$, much higher than those of undoped counterparts. More importantly, after Mo atom doping, the durability of the octahedra was also significantly improved, which can be confirmed by the fact that the specific activity of Mo-doped Pt_3Ni octahedra was only attenuated by 6.2% after 8000 cycles, while that of Pt_3Ni octahedra was decreased by 33%. The post-test characterizations showed that the loss of Ni atoms in Pt_3Ni was serious during the ORR electrocatalysis, while this phenomenon was obviously weakened after doping Mo atoms. In addition, the shape of the Mo-doped Pt_3Ni octahedra was well maintained after ORR durability tests, while the undoped octahedra became more spherical. Density functional theory (DFT) calculations revealed that Mo atoms tended to enhance the ORR performance by locating nearing the subsurface of the nanocrystal edge in vacuum and the surface vertex/edge sites under oxidation conditions.

The above research stimulated a series of works to explore the role of doping elements in improving the ORR activity and durability of catalysts. In view of the enhanced ORR performance of 1D Pt-based nanostructures compared with the 0D counterparts, Rh atoms were doped into ultrathin Pt nanowires with an average diameter of 1.3 ± 0.3 nm (Figure 4a) [118]. At 0.9 V (vs. RHE), the ORR specific and mass activities of Rh-doped Pt nanowires are 1.63 mA cm^{-2} and 1.41 A $mg_{Pt}{}^{-1}$, respectively, 1.2 and 1.6 times higher than those of pure Pt nanowires, respectively. More importantly, after 10,000 continuous cycles, the activity retention of Rh-doped Pt nanowires was 90.8%, much higher than that of Pt nanowires (80.5%), confirming that the durability had been significantly improved after Rh-doping (Figure 4b). The unique 1D anisotropic structure and the introduction of a small number of Rh atoms were the dominant reasons for the enhanced durability. In this respect, the incorporation of Rh atoms can suppress the dissolution of Pt atoms through preferentially sacrificing Rh atoms during long-term electrocatalytic tests, which can be confirmed by the fact that the atomic ratio of Pt/Rh was significantly decreased after 10,000 cycles, while Pt nanowires showed an obvious dissolution under the similar conditions. DFT

calculations revealed that the vacancy formation energy of Pt atoms in Rh-doped Pt models was obviously higher than in those without Rh atom doping, verifying that the enhanced durability can be achieved by improving the oxidation resistance of Pt atoms (Figure 4c). Similar observations were also found in Rh-doped Pt-based alloy systems [40,119]. Long-term durability tests made the shape of PtNi octahedral nanoparticles more spherical, while Rh doping can well maintain the octahedral shape, thus improving the ORR durability (Figure 4d) [119]. In terms of the PtNi nanowires, apart from maintaining the basic shape, the introduction of Rh atoms can substantially slow down the leaching of Ni atoms from nanowires [40]. Note that Rh atoms can further boost the vacancy formation energy of Ni atoms to reduce the leaching of Ni atoms from PtNiRh, on the basis of increasing the vacancy formation energy of Pt atoms.

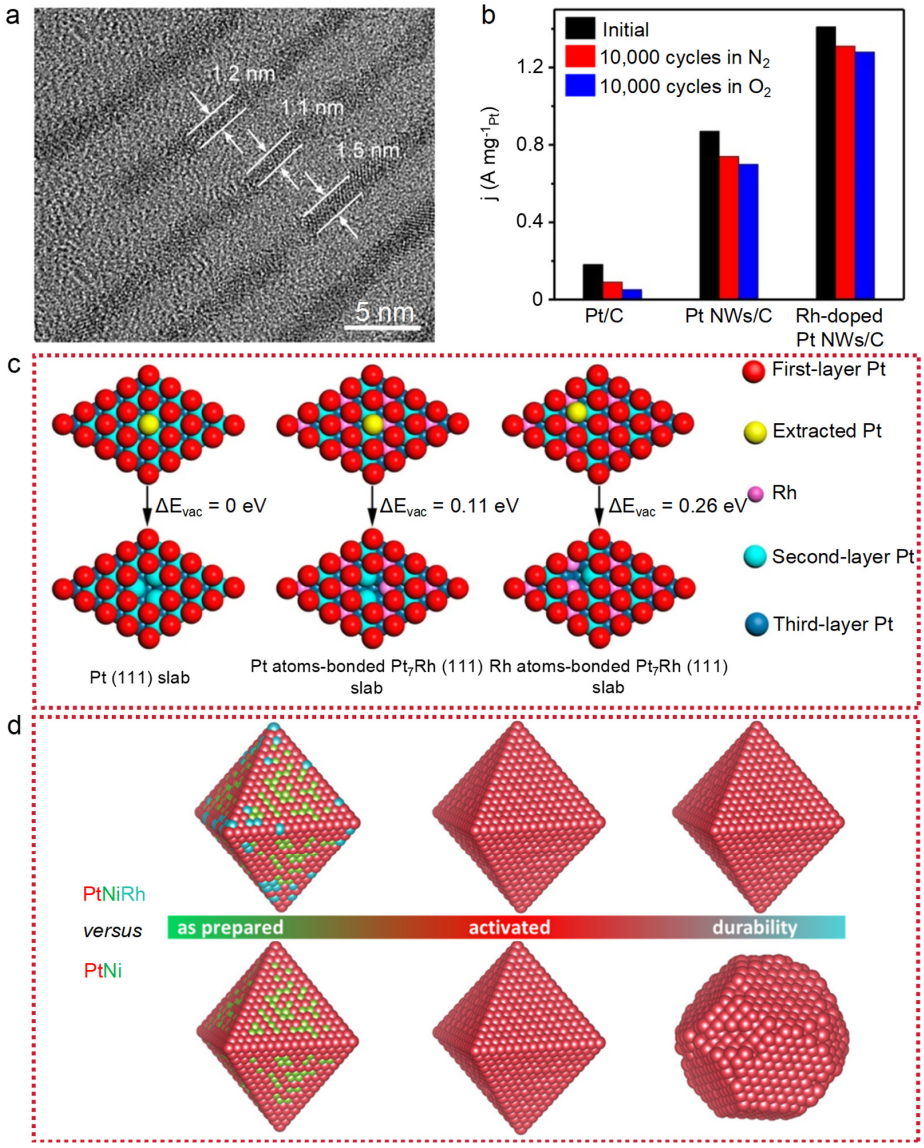

Figure 4. Enhancing ORR durability of Pt-based catalysts by Rh atoms doping. (**a**) Representative TEM image of ultrathin Rh-doped Pt nanowires. (**b**) The mass activities of Rh-doped Pt nanowires, Pt nanowires and commercial Pt/C catalysts after different potential cycles. (**c**) The Pt vacancy formation energy (ΔE_{vac}) of different models. Reprinted with permission from Ref. [118]. Copyright 2017 ACS. (**d**) The shape evolutions of PtNi octahedral nanoparticles with and without Rh atom doping during ORR electrocatalysis. Reprinted with permission from Ref. [119]. Copyright 2016 ACS.

It has been found that Ga atoms have a similar effect to the Rh atoms in terms of boosting the durability of Pt-based catalysts. Taking Ga-doped PtNi octahedral nanoparticles as an example, the doping of Ga atoms dramatically enhanced the ORR durability of PtNi octahedral nanoparticles, confirmed by the significantly improved activity retention after 30,000 cycles [120]. This conclusion was also reflected by the decreased ECSA of Ga-PtNi, decreased from 49 to 44 $m^2\ g_{Pt}{}^{-1}$, while that of PtNi was more obvious (28 $m^2\ g_{Pt}{}^{-1}$), because a small amount of surface Ga doping can effectively hinder the dissolution of Pt and Ni atoms from PtNi nanoparticles and the collapse of the preferred octahedral shape. Additionally, lavender-like Ga-doped Pt_3Co nanowires were rationally designed to further elucidate the key role of Ga atom doping in improving the ORR durability of Pt-based alloy catalysts (Figure 5a) [114]. The increase in the Ga atom content not only made the surface of the nanowires denser and denser, but also significantly improved the ORR durability of the nanowires. Among all kinds of nanowires, the half-wave potential of 8% Ga-doped Pt_3Co nanowires only decayed by 4 mV after 20,000 cycles, and the retention of the specific and mass activity was as high as 89.3% and 95.3%, respectively (Figure 5b). However, excessive Ga doping reduced the catalytic activity of Pt_3Co nanowires, putting forward a balance between the activity and durability by presenting an optimized idea. In this system, the decrease in the surface energy caused by Ga atom doping explained the enhanced durability of Pt_3Co nanowires (Figure 5c).

A strong metal bond can be formed by combining W atoms with Pt metal, which is extremely stable in an acidic environment, thus providing a new idea for W doping to enhance the ORR durability of Pt-based alloy catalysts [121,122]. To this end, W atoms served as an adhesive to stabilize the dissolution of transition metals from PtCu-based alloys (Figure 5d) [123]. After 30,000 durability tests, as-optimized $Pt_2CuW_{0.25}$ showed the lowest activity losses of 4.1% and 10.5% towards mass and specific activities, respectively, much superior to those of Pt_2Cu catalysts (Figure 5e). The enhanced durability of $Pt_2CuW_{0.25}$ mainly originated from the raised vacancy formation energy of Pt atoms caused by the stronger bonding between W and Pt/Cu atoms, leading to structural stability during the electrocatalytic tests (Figure 5f). This work presented a reasonable design to enhance the electrocatalytic durability by using high melting point metals to maintain the thermodynamic stability of Pt-based alloys. In addition, other high melting point metals can also act as dopants to improve the electrocatalytic durability, including Au, Ir and Re atoms, etc. [124–126]. Especially for the early transition metals, it has been found that alloying with Pt has been regarded as an efficient strategy to improve ORR performance [127]. Huang's group further introduced Re atoms into ternary PtNiGa ultrafine nanowires to construct a novel ORR catalyst with excellent activity, long-term stability and high atomic utilization [128]. The mass activity of as-optimized Re-doped PtNiGa nanowires was 19.6 times higher than that of commercial Pt/C, and the mass activity was only attenuated by 10.6% after 20,000 cycles. The optimal electronic structure of Re-doped PtNiGa nanowires caused the weakened binding strength towards oxygen-containing intermediates and elevated the dissolution potential, thus boosting the ORR activity and stability. More importantly, this catalyst also exhibited excellent performance as a cathode catalyst in the MEA tests, with a peak power density of 961 mW cm^{-2} and a current density decrease of only 4.9% after a discharge voltage of 0.75 V for 100 h.

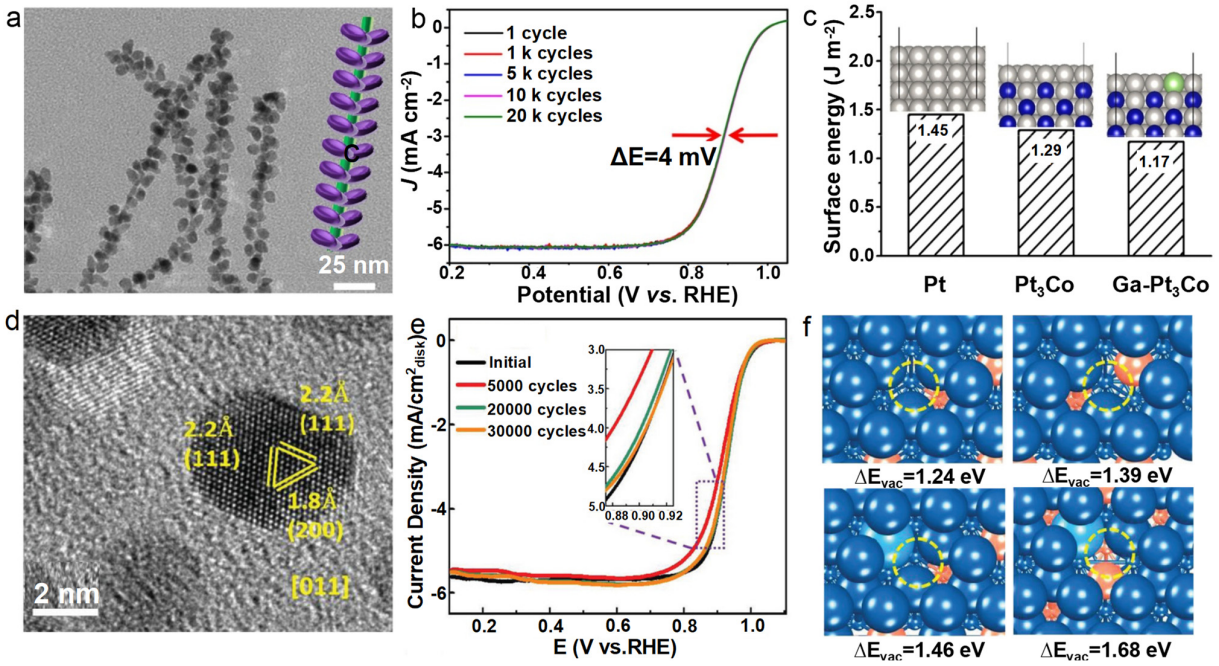

Figure 5. Enhancing ORR durability of Pt-based catalysts by other metal atom doping. (**a**) Representative TEM image and the corresponding schematic illustration of 4% Ga-doped Pt_3Co nanowires. (**b**) ORR polarization curves of 8% Ga-doped Pt_3Co nanowires before and after different potential cycles. (**c**) Surface energy and ΔE_0 of the pure Pt, Pt_3Co and Ga-doped Pt_3Co (111) surfaces (the insets are the corresponding computational models, and the gray, blue and green spheres represent Pt, Co and Ga atoms, respectively). Reprinted with permission from Ref. [114]. Copyright 2020 ACS. (**d**) Representative HRTEM image of $Pt_2CuW_{0.25}$ nanoparticles. (**e**) ORR polarization curves of $Pt_2CuW_{0.25}$ nanoparticles before and after different potential cycles (*inset* is the partial enlargement). (**f**) Structures of Pt vacancies formed on different sites of the PtCu (111) or PtCuW (111) surfaces and the corresponding ΔE_{vac} values (the yellow circles are the locations of the vacancies, the Pt, Cu and W atoms are shown in dark blue, orange and light blue). Reprinted with permission from Ref. [123]. Copyright 2020 Wiley.

In addition to the transition metal doping engineering, the designs of light element doping are also of great interest for stabilizing the dissolution of Pt and transition metals during the long-term ORR cycles, such as F, H, N, P and B [129,130]. Among these light element-doped Pt-based alloys, light elements tend to occupy the largest available gap position to form interstitial alloys rather than substitute alloys. In contrast to traditional alloys, such interstitial alloys maintain the lattice structure of the original alloy to the greatest extent, which can optimize the electronic structure of surface-active sites through strong orbital hybridization, thus enhancing the activity and durability of the catalysts. B atoms have been interstitially doped into 3 nm Pt nanoparticles with a doping amount of 6.6% to improve the ORR activity and durability of Pt nanoparticles [131]. Due to the doping of interstitial B atoms, the half-wave potential was only decreased by 5 mV after 10,000 cycles, superior to that of pure Pt nanoparticles, with a decreased half-wave potential of 23 mV. In addition, under H_2-O_2 fuel cell conditions, the MEA with B-doped Pt nanoparticles as cathodic catalysts showed a smaller attenuation in the power density compared with that based on Pt nanoparticles. Theoretical calculations indicated that the downshift of the *d*-band center caused by the interstitial doping of B atoms suppressed the oxidative disruption of surface Pt atoms, thus enhancing the ORR durability.

4.3. Core/Shell Structures

Since only the surface atoms of the catalysts can contact the electrolyte to participate in the reactions, Pt-based core/shell structures with a high Pt utilization have been widely

developed, especially those with low-cost cores and a thin layer of catalytically active shells [132–134]. Generally, the cores will not take part directly in electrocatalysis, *yet* they play an indispensable role in affecting the performance of the active shells through the potential strain and/or ligand effects. In the case of the mismatched lattice between the core and shell, the strain effect becomes more obvious compared with solid solution alloy counterparts, which is significantly important for regulating the electrocatalytic performance [135,136]. More importantly, the overlayers on cores can also improve the durability by inhibiting the loss of transition metals in the overall core/shell catalysts.

The core/shell structures with a Pt monolayer are the most classical catalysts to mitigate the drawbacks of traditional alloy catalysts, which can provide ultralow Pt loading and ultrahigh Pt utilization, as well as the possibility of optimizing the catalytic performance by the interactions between the overlayers and metal or alloy cores [137]. Sasaki et al. designed a kind of highly durable ORR electrocatalyst composed of Pt monolayers on PdAu alloy nanoparticles (Pt_{ML}/PdAu) (Figure 6a) [138]. After testing for as long as 100,000 cycles under fuel cells, as-designed Pt_{ML}/PdAu showed an attenuation of ~8% in terms of its mass activity, much more excellent than those of Pt_{ML}/Pd and commercial Pt/C (Figure 6b). The introduction of Au atoms into the core made the Pt monolayer significantly tolerant, thus showing a high durability towards ORR electrocatalysis and being very promising for the practical fuel cells. Driven by these unique core/shell structures with Pt monolayers, the catalysts with a Pt-skin structure were further presented to inhibit the dissolution of transition metals internally [139,140]. By replacing the Cu atoms in three surface layers of the AuCu intermetallics by Pt atoms, a Pt skin on a AuCu intermetallic catalyst can be elaborately designed, which can maximize the Pt utilization to enhance ORR activity and durability (Figure 6c) [141]. The theoretical calculations showed that the Pt-skin structure composed of a 1.5 Pt-skin layer on a AuCu (111) substrate can display a weakened oxygen affinity compared with that on Pt (111), thus contributing to more favorable ORR electrocatalysis (Figure 6d). In fact, most Pt-based catalysts prepared by annealing or activated under acidic conditions are likely to form a Pt-skin surface, which is generally caused by atomic segregation under high temperature and the loss of surface transition metals [57,140,142]. In this part, we only discuss the elaborate Pt-skin core/shell catalysts, while neglecting the spontaneously formed Pt-skin structures.

Beyond core/shell catalysts with Pt-skin layers, several new attempts were further presented to optimize the ORR performance of Pt-based core/shell catalysts, including doping foreign atoms into cores, adjusting the thickness of shells, tuning the composition of the core and/or shell and morphology-controlled core/shell structures [143,144]. In terms of doping engineering, anion doping has been regarded as an efficient strategy to enhance the ORR activity and durability. This is because of the fact that the doping of anions can not only provide the optimal strain fields for surface Pt atoms, but also form chemically stable cores by reacting with selected elements. For example, a high-pressure nitriding strategy was conducted to adjust the doping amount of N atoms in PtCo core/shell nanoparticles, aiming at maintaining the electrochemical surface area to further improve the ORR stability (Figure 6e) [145]. Compared with commercial Pt/C, the mass activity and durability of N-PtCo core/shell catalysts were enhanced by two times and five times, respectively. After 180,000 cycles, the mass activity of N-PtCo core/shell catalysts can still retain 80% of the initial activity, and the core/shell structure can be well maintained after 1,000,000 cycles. In this system, the higher concentration of N atoms in core/shell nanoparticles is more favorable through optimizing the oxygen binding energy on the Pt surface and preventing the dissolution of Pt/Co atoms.

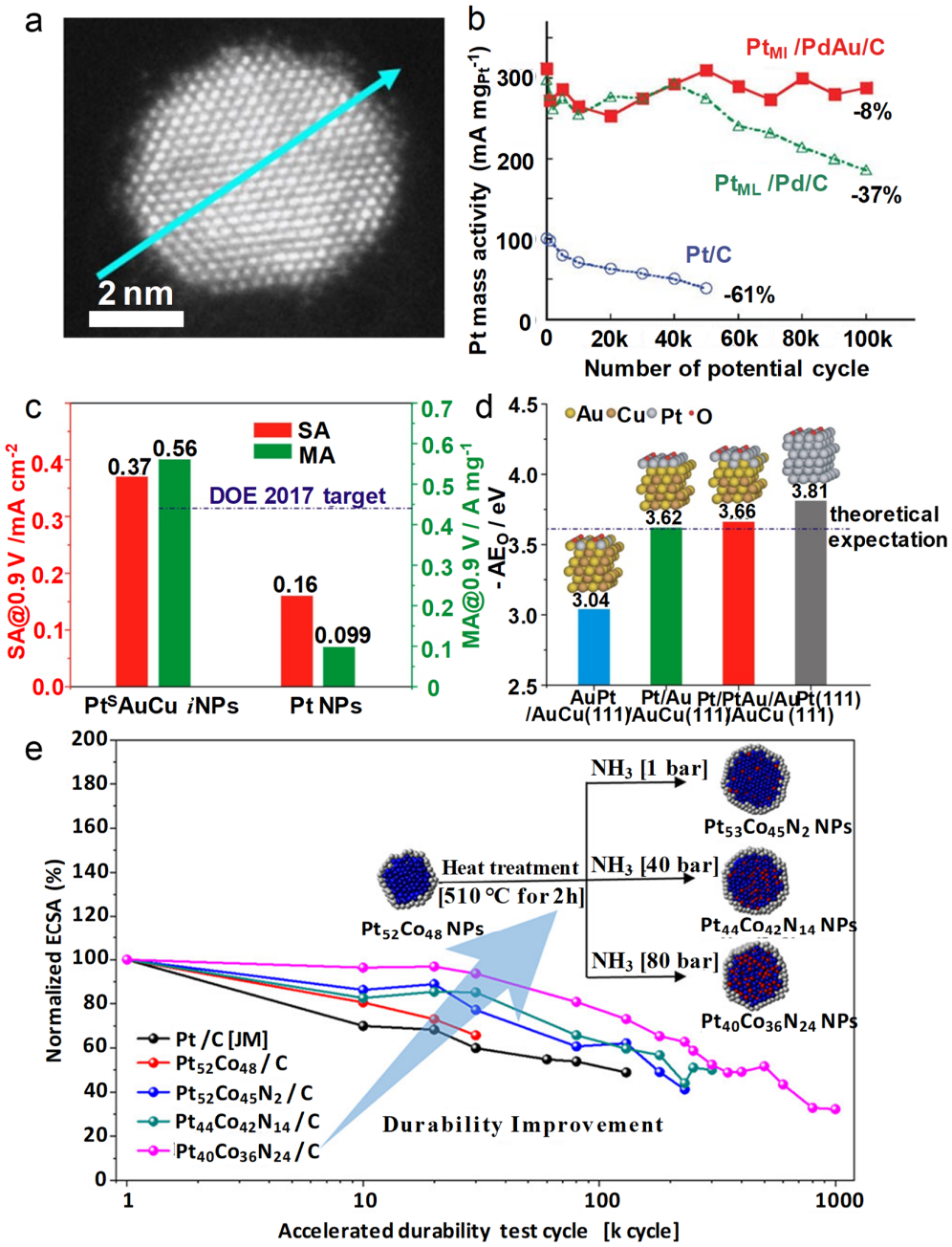

Figure 6. Enhancing ORR durability of Pt-based catalysts by core/shell nanoparticles. (**a**) HAADF-STEM image and the corresponding line-scan result of carbon-supported Pt_{ML}/Pd_9Au_1 nanoparticles. (**b**) The mass activities of the Pt_{ML}/Pd_9Au_1, Pt_{ML}/Pd and Pt/C catalysts after different potential cycles. Reprinted with permission from Ref. [138]. Copyright 2012 Springer Nature. (**c**) The specific and mass activities of Pt-skin AuCu and Pt nanoparticles. (**d**) Oxygen adsorption energy (ΔE_O) for AuCu(111) surfaces covered with different thicknesses of Pt skin and Pt (111) surface. Reprinted with permission from Ref. [141]. Copyright 2014 ACS. (**e**) The normalized ECSA values of PtCo core/shell nanoparticles with different doping amount of N atoms after different potential cycles (insets are the corresponding atomic models). Reprinted with permission from Ref. [145]. Copyright 2021 ACS.

Strain and ligand engineering are the most common effects in core/shell structure catalysts, which can optimize the catalytic activity by regulating the electronic structure of surface atoms [146–148]. In fact, when the shell thickness is less than three atomic layers, the ligand and strain effect jointly dominate the electrocatalytic performance, while the ligand effect disappears beyond three atomic layers [135,149]. Note that the bifunctional effect will

be reflected in the core/shell catalysts with the further increase in shell thickness. Hence, the shell thickness plays an important role in enhancing the ORR activity and durability of core/shell catalysts, and the optimized thickness of Pt layers required to obtain the optimal performance may depend on the properties of the cores. In order to search the optimal Pt-layer thickness for ORR electrocatalysis, DFT calculations were conducted to study the influence of Pt-layer thickness on various $L1_0$-PtM (M = V, Cr, Fe, Co, Ni and Cu) catalysts on the oxygen binding energy [150]. It was found that the oxygen binding energy decreased with the increase in Pt-shell thickness, leading to the improved catalytic performance, making the Pt–M catalyst with three Pt layers display a better ORR activity than those with one or two Pt layers. Experimentally, Pt layers were deposited on the corners and (100) terraces of the Pd nanocubes (Pt_{corner}/Pd_{NC} and $Pt_{terrace}/Pd_{NC}$), and the corrosion kinetics were further studied using in situ transmission electron microscopy (TEM) [132]. The corners of Pt_{corner}/Pd_{NC} were protected by Pt layers, inhibiting the etching of the overall particles, thus boosting the durability of the catalysts. However, the $Pt_{terrace}/Pd_{NC}$ exhibited a preferential dissolution at the corner of Pd_{NC} to show a low catalytic durability during ORR tests.

Constructing the Pt-based alloy shells on the cores is another effective strategy to reduce the cost of Pt-based core/shell catalysts and further improve the ORR activity and durability. Combining the Au cores and PtCo-based shells, the ORR durability was significantly improved, which was mainly due to the strong electronic interaction of subsurface segregated Au atoms [151]. The well-designed Au-core@Co-interlayer@PtCoAu-shell multilayer structure showed the specific activity of 1.730 mA cm^{-2} and mass activity of 0.692 A $mg_{Pt}{}^{-1}$, 7.0 and 4.0 times higher than those of commercial Pt/C catalysts, respectively. More importantly, the activity loss for the multilayered catalyst was only 6.14% while that of the commercial Pt/C exceeded 35%. Therefore, the alloy shell can also overcome the problem of composition loss by optimizing the electronic structure of surface Pt atoms and finely designing the composition distribution to enhance the electrocatalytic durability.

Considering that the multidimensional structures can provide a strong interaction with supports to induce the well's structural stability, the Pt-based core/shell structures with an anisotropic morphology will be the ideal platforms to obtain excellent ORR durability [152–154]. Although segregated Pt-skin structures are extraordinarily active towards ORR electrocatalysis, this is difficult to achieve on the surface of nanocrystals with high-index facets [88,142,155]. To address this challenge, Guo et al. achieved the highly active and stable Pt-skin surface with high-index facets via annealing the presynthesized Pt_3Fe zigzag-like nanowires under H_2/Ar environments (Figure 7a–c) [142]. The unique nanowire morphology and Pt-skin surface enable as-prepared Pt-skin Pt_3Fe nanowires to have an extremely high ORR mass activity of 2.11 A $mg_{Pt}{}^{-1}$ and specific activity of 4.34 mA cm^{-2}. More importantly, high-index facets enclosed Pt-skin Pt_3Fe nanowires were also electrochemically stable under harsh electrocatalytic conditions with a little mass activity decay of 24.6%, *yet* the pristine Pt_3Fe nanowires showed serious activity decay, especially after a long-term cycle (Figure 7d,e). The optimal oxygen adsorption energy induced by the combination of a strong ligand and strain effect dominated the enhanced ORR performance, revealed by the density functional theory calculations (Figure 7f). In addition, the Pt-skin Pt_3Fe nanowires also showed a high resistance to morphological and structural transformations during ORR electrocatalysis, and can protect favorable Fe atoms from being dissolved, thus maintaining a high activity under operating conditions. This strategy can further extended into PtCo zigzag-like nanowires, which showed a Pt-skin surface with high-index facets and high electrocatalytic performance [156]. Recently, the mesoporous Pt/Pt-skin Pt_3Ni core/shell framework nanowires were designed to finely integrate the anisotropic advantages of 3D porous nanoframes and 1D nanowires (Figure 7g) [157]. This catalyst was composed of 1D ultrafine Pt nanowires (~3 nm) and mesoporous Pt-skin Pt_3Ni framework (Figure 7h), which has displayed excellent ORR activity and durability, as well as ultrahigh Pt atom utilizations. Surprisingly, the well-designed Pt/Pt-skin Pt_3Ni

core/shell framework nanowires exhibited an ultradurable stability, with the activity less than 3% after continuous 50,000 cycles (Figure 7i).

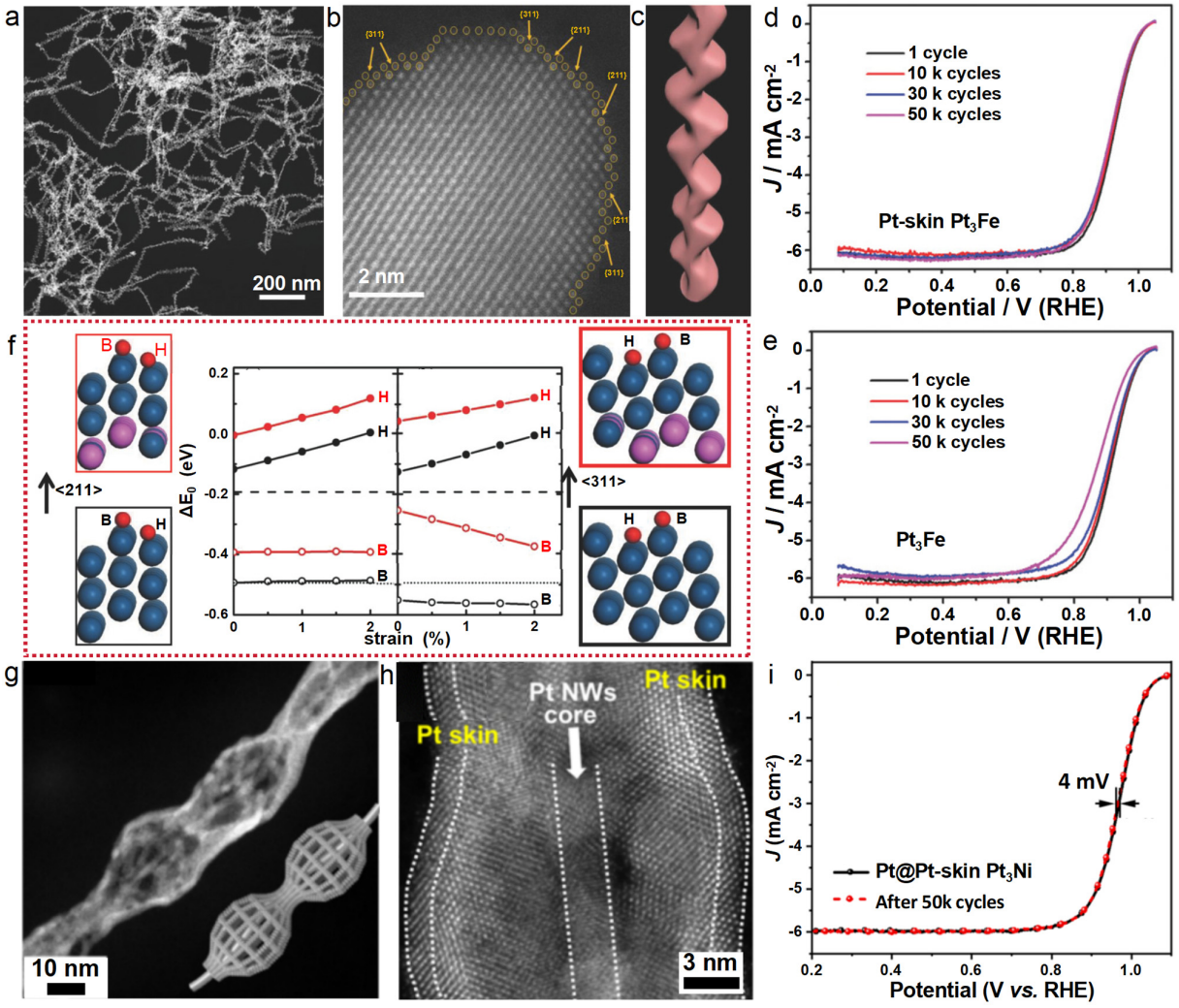

Figure 7. Enhancing ORR durability of Pt-based catalysts by core/shell nanostructures with anisotropic morphologies. Representative (**a**) low- and (**b**) high-magnification HAADF-STEM images of Pt-skin Pt_3Fe zigzag-like nanowires. (**c**) Structural illustration of the Pt-skin Pt_3Fe zigzag-like nanowire. ORR polarization curves of (**d**) Pt-skin Pt_3Fe and (**e**) pristine Pt_3Fe zigzag-like nanowires before and after different potential cycles. (**f**) DFT calculations of oxygen adsorption energy on different models. Reprinted with permission from Ref. [142]. Copyright 2018 Wiley. (**g**) Representative HAADF-STEM and (**h**) HRTEM images of mesoporous Pt/Pt-skin Pt_3Ni core-shell framework nanowires. (**i**) ORR polarization curves of mesoporous Pt/Pt-skin Pt_3Ni core-shell framework nanowires before and after ORR durability tests. Reprinted with permission from Ref. [157]. Copyright 2023 Springer Nature.

Two-dimensional Pt-based core/shell nanocrystals are also ideal catalyst models to achieve highly durable ORR electrocatalysis. A typical example is the biaxially strained PtPb/Pt core/shell nanoplates synthesized using a one-step wet-chemical method [158]. The PtPb/Pt core/shell nanoplates showed a side length of about 16 nm and a thickness of 4.5 ± 0.6 nm, where two different interfaces, the (010) PtPb//(110) Pt interface between PtPb core and edge Pt shell and the (001) PtPb//(110) Pt interface between PtPb core and top (bottom) Pt shell, exist. The top Pt layer was completely connected with the PtPb core, resulting in a tensile strain of 7.5% along $[100]_{Pt}$ and a compressive strain of 11% along $[01\text{-}1]_{Pt}$. On the other hand, in the edge Pt layer, the [001] direction of Pt was

completely restricted, resulting in a 7.5% tensile strain and very small compressive strain along $[110]_{Pt}$. In this catalytic system, a compressive strain can weaken the Pt–O binding energy on the surface of Pt (111) and promote the ORR activity. The tensile strain was beneficial for optimizing the low-coordination atoms with strong Pt–O bonds to enhance the ORR properties. Therefore, the resulting biaxial strain effect made the PtPb/Pt core/shell nanoplates show a much better ORR catalytic activity and durability than the commercial Pt/C and PtPb nanoparticles.

4.4. Intermetallics

Over the past decade, Pt-based intermetallics have been extensively studied as electrocatalysts for fuel cell devices, which is due to their lower negative entropy and stronger electronic interaction between different atoms [159–161]. In light of the strong *d*-orbital interaction between different atoms originated from the sufficient atomic acquaintance within an alternated distribution, the promoted ligand effect and obviously downshifted *d*-band center have been observed on various Pt-based intermetallics [162–164]. The regulation of the electronic structure enables the optimized adsorption/desorption towards oxygenated intermediates, thus contributing to the enhanced ORR electrocatalysis. In addition, the different lattice compressive strains will be caused by the highly spaced atoms with different radii, further optimizing the energy band structure of nanocrystals. More importantly, in terms of durability, the excessive corrosion under harsh ORR conditions can be prevented by the close combination of alloying elements originated from the intrinsic ordered structure and strong atomic interaction of intermetallics, thus endowing Pt-based intermetallics with a high ORR durability.

Owing to the unique structural characteristics of intermetallics, the significantly enhanced ORR activity and durability have been observed on various Pt-based intermetallic nanocrystals [140,165–169]. For instance, the core/shell $L1_0$-CoPt/Pt nanoparticles with an intermetallic structure showed a higher ORR activity and durability than the disordered counterparts [168]. The intermetallic CoPt/Pt nanoparticles were synthesized via annealing the cashew-like CoPt nanoparticles at 650 °C (Figure 8a). In this structure, the core exhibited alternative layers of Pt and Co atoms, and the shell was 2–3 atoms thick of Pt, thus providing a stronger ability to protect the acidic etching of Co atoms (Figure 8b). As a result, a high mass activity of 0.56 A mg_{Pt}^{-1} and excellent durability with a negligible activity loss after 30,000 cycles can be achieved on the intermetallic CoPt/Pt nanoparticles (Figure 8c), while the disordered A1-CoPt nanoparticles showed a 41% drop in the mass activity under the same cycle conditions. Note that the cashew-like shapes cannot be well maintained despite the conversion from a disordered to intermetallic $L1_0$ structure, because of the unavoidable nanocrystal aggregation induced by Ostwald ripening under high-temperature conditions. Therefore, the rational selection of synthetic methods to avoid sintering and aggregation is vital for further optimizing the ORR performance through limiting the particle sizes and narrowing the size distributions.

Several typical strategies have been presented to avoid the agglomeration during annealing treatment, such as shell-protected annealing [170], oxide-driven atomic ordering [167,171], matrix protection methods [172], and nanoconfinement strategies [173–175], etc. Herein, we take two typical examples to clarify the size control of these methods and the significance towards the enhanced electrocatalytic performance. The first one is to anneal Pt nanoparticles encapsulated in a ZnO matrix at 600 °C for 2 h under a H_2/Ar atmosphere to achieve the ordering of PtZn intermetallic nanoparticles, after which the excess ZnO matrix was removed through acidic treatment (Figure 8d) [176]. The ZnO matrix can not only be partially reduced to Zn atoms to interdiffuse with Pt atoms to form intermetallics, but also prevent the further sintering and agglomeration of nanoparticles during annealing processes. The biaxial strain of Pt shells with 3.9% compression along the <011> and <101> directions and 2.23% tension along the <110> direction was achieved on PtZn intermetallic nanoparticles (Figure 8e,f), thus leading to an optimal oxygen adsorption energy (Figure 8g). The biaxially strained PtZn intermetallic nanoparticles displayed a high

mass activity of 1.02 A mg_{Pt}^{-1} and a specific activity of 1.68 mA cm^{-2}, as well as excellent durability with a negligible activity attenuation after 10,000 cycles (Figure 8h). In contrast, the disordered PtZn nanoparticles suffered from severe degradation with a downshifted half-wave potential of 15 mV.

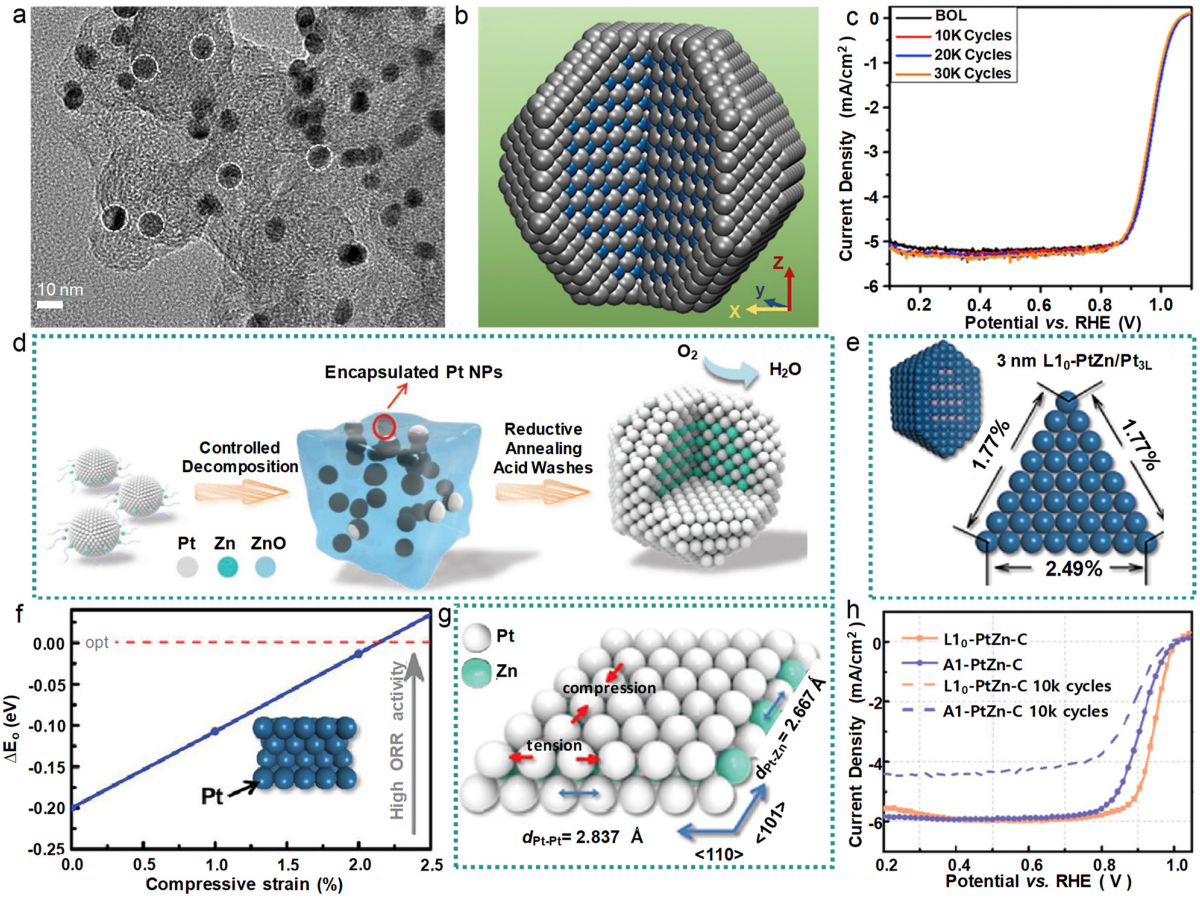

Figure 8. Enhancing ORR durability of Pt-based catalysts by intermetallic nanoparticles. (**a**) Representative TEM image and (**b**) structural illustration of core/shell $L1_0$-CoPt/Pt nanoparticles. (the silver color atom is Pt and the blue color atom is Co) (**c**) ORR polarization curves of core/shell $L1_0$-CoPt/Pt nanoparticles before and after different potential cycles. Reprinted with permission from Ref. [168]. Copyright 2019 Elsevier. (**d**) Schematic illustration of the synthesis of $L1_0$-PtZn/Pt nanoparticles. (**e**) Schematic illustration of biaxial strain between $L1_0$-PtZn core and A1-Pt shell. (**f**) Simulation model of 3 nm $L1_0$-PtZn/Pt_{3L} nanoparticle and strain distribution on the (111) surface of the $L1_0$-PtZn/Pt nanoparticle. (**g**) ΔE_O of compressive strain on the Pt (111) surfaces. (**h**) ORR polarization curves of $L1_0$-PtZn and A1-PtZn nanoparticles before and after 10,000 cycles. Reprinted with permission from Ref. [176]. Copyright 2020 Wiley.

In addition, Liang et al. presented a sulfur-anchoring strategy for achieving the strong interaction between Pt and S atoms in the carbon matrix to suppress the sintering of nanoparticles even at annealing temperatures up to 1000 °C, thus being a promising method to prepare small-sized Pt-based intermetallic nanoparticles [177]. In light of the advantages of the sulfur-anchoring approach, a Pt-based intermetallic (PtM, Pt_3M and PtM_3) library can be constructed, demonstrating the possibility of the general synthesis of small-sized intermetallic nanoparticles by escaping from the trouble of simultaneously accelerated interparticle sintering dynamics and the intraparticle atomic order dynamics with the increased temperature. The optimized intermetallic PtCo nanoparticles showed the highest ORR activity among the prepared Pt-based intermetallics, and their potential application in practical H_2-air fuel cells with an ultralow Pt loading of 0.02 mg_{Pt} cm^{-2} and a maximum power density of 1.08 W cm^{-2}. To this end, transforming disordered

nanocrystals into ordered intermetallics has been considered as a promising way to improve the ORR activity and durability of Pt-based catalysts.

Pt-based ternary intermetallics constructed by introducing an additional element into Pt-based ternary systems seem to be a long-awaited answer to further improve the catalytic durability. Through synthesizing a series of $L1_0$-PtMCo (M = Mn, Fe, Ni, Cu and Zn) nanoparticles, the optimal position of the theoretical volcano plot was successfully achieved due to the anisotropic strain levels on distorted Pt (111) surfaces [178]. Among various PtMCo intermetallic nanoparticles, the $L1_0$-PtNiCo nanoparticles showed the highest ORR activity of 3.1 A mg_{Pt}^{-1} and 9.3 mA cm^{-2}. In terms of durability, the mass activity loss of $L1_0$-PtNiCo nanoparticles was only 15.9% after 30,000 cycles, demonstrating the enhanced ORR performance on ordered Pt-based ternary systems.

Shape-controlled synthesis of intermetallics has always been a research hotspot but has only displayed limited success. This is mainly because of the fact that the necessary annealing conditions will break and coarsen the pristine nanocrystals, thus necessitating the robust initial structures or relatively low annealing temperatures. In this case, a shell-protected annealing strategy may be an efficient strategy to maintain the initial anisotropic structures when using the robust nanocrystals as precursors [179–181]. Taking the PtFeIr nanowire as an example, the use of SiO_2 shells can alleviated the breakage, aggregation and sintering of initial nanowires during annealing (Figure 9a) [179]. Without the protection of SiO_2, PtFeIr nanowires will be transformed into nanoparticles under such a harsh annealing environment. However, such an ordered phase transformation with negligible shape change is still highly dependent on the robust thermally stable precursors, confirmed by the fact that the SiO_2-protected PtFe nanowires would be broken into nanoparticles under the same annealing conditions. This is because that the existence of Ir with a high melting point was beneficial for the maintenance of 1D nanostructures by improving the thermal stability of nanowires. Combining the advantages of ordered intermetallics and 1D nanostructures, as-prepared ordered PtFeIr nanowires show a high ORR activity, with a specific activity of 2.40 mA cm^{-2} and a mass activity of 2.03 A mg_{Pt}^{-1}, as well as the minimum activity loss after 10,000 cycles (Figure 9b).

An important method for controlling the anisotropic morphology of nanocrystals is template method, which has been extended to the preparation of intermetallic nanocrystals. The template method can be further divided into the soft-template method and hard-template method. The former mainly uses ordered aggregates formed by amphiphilic molecules as soft templates to control the shape of nanocrystals. To this end, various Pt-based intermetallic nanoplates have been synthesized by using the reasonably selected surfactants, including PtPb, PtBi and nanoplates [158,182]. In addition, the hard-template method can be used to construct the mesoporous materials via introducing the metal precursors into the hard-template channels. The subsequent roasting and template removal make the corresponding mesoporous materials become possible. The KIT-6 templates have been used to create various Pt-based intermetallic mesoporous nanocrystals [183]. A typical example is the preparation of ordered mesoporous intermetallic Ga–Pt (*meso-i*-Ga–Pt) nanoparticles through synergizing the anion induction and concurrent template methods (Figure 9c) [184]. As-prepared *meso-i*-Ga-Pt nanoparticles presented a uniform and monodisperse polyhedron-like morphology, and the mesoporous channels run through the whole nanoparticles in an inversed double-gyroid structure (Figure 9d). Benefiting from the unique structures of *meso-i*-Ga_1Pt_1 nanoparticles, a high ORR mass activity of 66.7 A g_{Pt}^{-1} can be achieved in 0.1 M KOH, much higher than those of *meso-i*-Ga_3Pt_5, *meso*-Pt and commercial Pt/C. In addition, after 15,000 cycles, the activity decline was only 47%, and the basic structures could be well maintained, indicating the excellent durability of *meso-i*-Ga_1Pt_1 nanoparticles (Figure 9e). The surface electronic structure analysis and DFT calculations revealed that the high ORR performance of *meso-i*-Ga_1Pt_1 was mainly caused by the arrangement of chiral atoms and the abundance of exposed Pt sites, which is beneficial to the optimization of the adsorption/desorption towards reactants and the optimal Gibbs free energy of ORR electrocatalysis (Figure 9f,g).

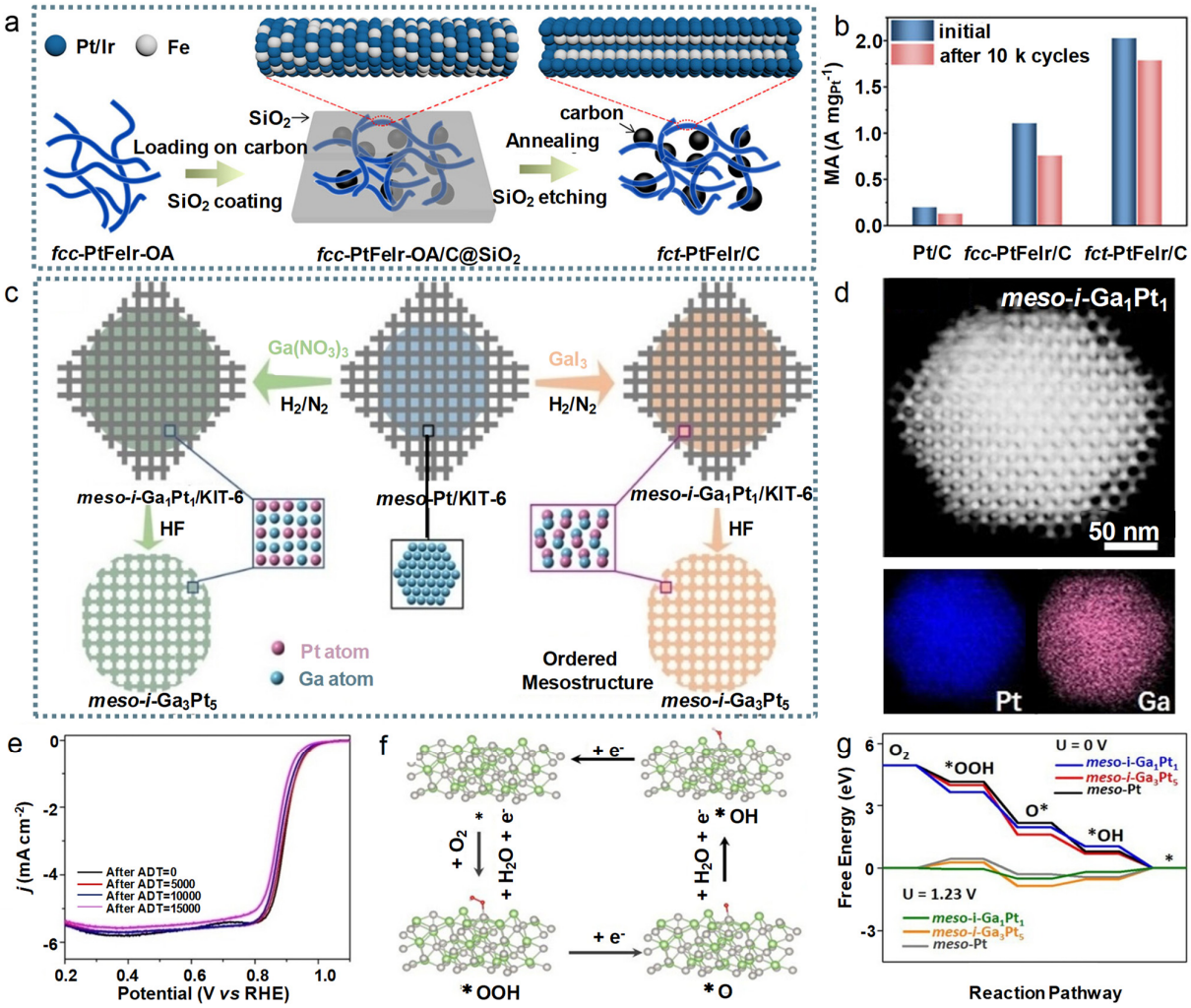

Figure 9. Enhancing ORR durability of Pt-based catalysts by intermetallic nanostructures with anisotropic morphologies. (**a**) Schematic illustration for the synthesis of *fct*-PtFeIr nanowires through the silica-protected strategy. (**b**) The mass activities of *fct*-PtFeIr nanowires, *fcc*-PtFeIr nanowires and commercial Pt/C catalysts before and after 10,000 cycles. Reprinted with permission from Ref. [179]. Copyright 2022 Wiley. (**c**) Schematic illustration for the synthesis of ordered *meso-i*-Ga-Pt nanoparticles with precisely controlled intermetallic phases induced by different Ga salts (NO_3^- and I^-). (**d**) Representative HAADF-STEM image and the corresponding elemental mappings of ordered *meso-i*-Ga-Pt nanoparticle. (**e**) ORR polarization curves of ordered *meso-i*-Ga-Pt nanoparticles before and after different potential cycles. (**f**) Configurations of adsorbed intermediates (*OOH, *O and *OH) ordered *meso-i*-Ga-Pt nanoparticles. (**g**) ORR pathways for *meso-i*-Ga_1Pt_1, *meso-i*-Ga_3Pt_5 and *meso*-Pt nanoparticles summarized at U = 0 V and 1.23 V. Reprinted with permission from Ref. [184]. Copyright 2023 Wiley.

It has been found that the ORR performance of Pt-based intermetallics is also highly dependent on the ordering degree [168,185,186]. Generally, the ORR activity and stability will be enhanced with the increase in the ordering degree [185,187]. However, most reported Pt-based intermetallic electrocatalysts tend to show a low ordering degree, challenging the further enhancement of ORR activity and durability. In order to obtain highly ordered PtCo-based intermetallics, Liang's group presented a low-melting-point metal (M = Ga, Pb, Sb and Cu) doping strategy to boost the ordering degree (Figure 10a) [188]. Owing to the decreased atom diffusion energy barrier caused by the low-melting-point metal doping, the ordering degree of the M-doped PtCo intermetallics increases with the decrease in the melting point of M (Figure 10b). The optimized Ga-doped PtCo intermetallics not

only showed superior ORR performance in a half-cell environment, but they can also be used as high-efficient cathodic catalysts for the practical fuel cells. A high mass activity of 1.07 A mg_{Pt}^{-1} at 0.9 V in H_2-O_2 fuel cells and a peak power density of 1.05 W cm^{-2} in H_2-air fuel cells can be achieved, far exceeding the US Department of Energy (DOE) 2025 target (Figure 10c). Due to the high ordering degree, the Ga-doped PtCo intermetallics cathode still maintained a high mass activity of 0.88 A mg_{Pt}^{-1} with an attenuation of 17.8%. This work not only put forward an effective strategy to regulate the ordering degree of intermetallics, but also highlighted the importance of foreign metal doping in intermetallics for boosting the catalytic performance.

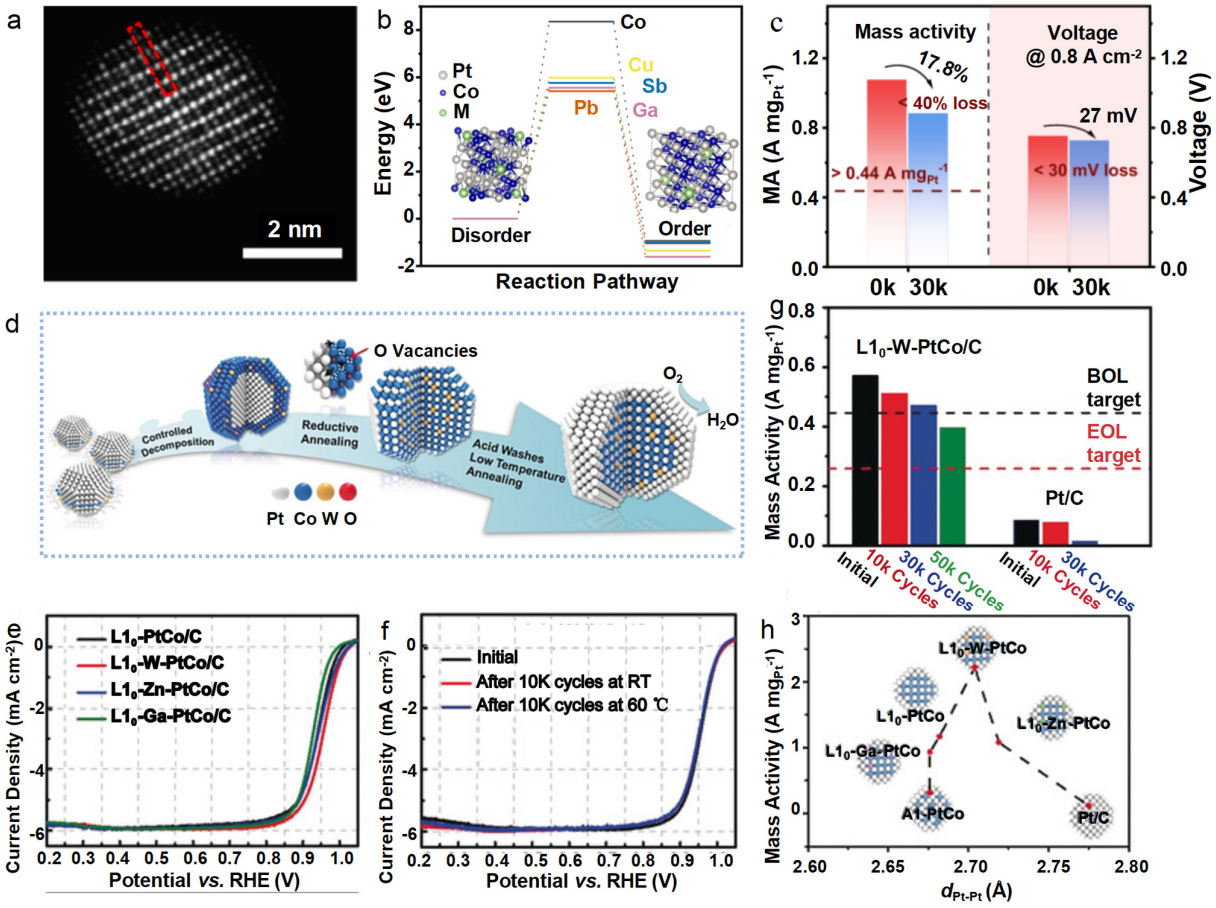

Figure 10. Enhancing ORR durability of Pt-based catalysts by combining the intermetallics and doping engineering. (**a**) Representative HAADF-STEM image of ordered Ga-doped PtCo intermetallic nanoparticle. (**b**) The disorder–order phase transition energy barrier of the low-melting-point metal doping PtCo nanoparticles (insets are the atomic model for disordered and ordered M-doped PtCo nanoparticle). (**c**) The mass activities at 0.9 V in H_2-O_2 fuel cell and the voltage at 0.8 A cm^{-2} in H_2-O_2 fuel cell before and after durability tests. Reprinted with permission from Ref. [188]. Copyright 2023 Springer Nature. (**d**) Schematic illustration for the synthesis of W-doped PtCo intermetallic nanoparticles. (**e**) ORR polarization curves of $L1_0$-PtCo with different metal doping. (**f**) ORR polarization curves of $L1_0$-W-PtCo intermetallic nanoparticles before and after durability tests at room temperature and 60 °C. (**g**) Mass activity of $L1_0$-W-PtCo/C and Pt/C at 0.9 $V_{iR\text{-}free}$ before and after voltage cycles at 80 °C under practical fuel cell conditions (black and red dash lines indicate the DOE beginning-of-life (BOL) and end-of-life (EOL) targets, respectively). (**h**) Correlations between ORR mass activities and Pt–Pt band distance of different catalysts. Reprinted with permission from Ref. [71]. Copyright 2019 Wiley.

In the case of doping engineering, a small number of W, Ga and Zn atoms was introduced into the PtCo intermetallic nanoparticles derived from the core/shell Pt/CoO_x

nanoparticles [71]. The introduction of the third metals was achieved via simply mixing the appropriate amounts of third metal precursors with Co precursors during the synthesis process (Figure 10d). Among all kinds of metal-doped PtCo intermetallics, W-doped PtCo intermetallic nanoparticles showed the highest ORR mass activity of 2.21 A $mg_{Pt}{}^{-1}$ and specific activity of 3.60 mA cm^{-2}, as well as the negligible activity loss after 10,000 cycles under both room temperature and 60 °C (Figure 10e,f). In light of the superior activity and durability of the W-doped PtCo intermetallic nanoparticles, the nanoparticles can be served as cathodic catalysts for fuel cells, which can achieve an initial mass activity of 0.57 A $mg_{Pt}{}^{-1}$ and only a 70% activity loss after 50,000 cycles (Figure 10g). In this system, the desired compressive strain and reduced surface energy of Pt surface caused by W atom doping in an ordered intermetallic structure are the dominant reasons for high activity and durability (Figure 10h).

As discussed in the previous section, the core/shell nanocrystals have shown the improved electrocatalysis through the adjustable electronic structure of the surface environment caused by the potential strain and ligand effect. During the thermal treatment process, as the common preparation strategy for intermetallics, it is easy to form a Pt-skin shell, which is mainly due to the migration of metal atoms under a high-temperature environment [167,178]. The favorable compressive strain can be generated by the thin shells, thus achieving the shift down of the *d*-band center to enhance the electrocatalytic performance. In addition, the unique electrocatalytic properties can be further generated by deliberately designing Pt-based intermetallics with core/shell structures, which mainly derives from the difference of core or shell with intermetallic structures [189,190]. A noteworthy catalyst platform is one where both the core and shell are replaced by different intermetallics [189]. The PtBi intermetallic shells that were 2–3 ordered layers thick were covered on annealed carbon-supported FePt intermetallic nanoparticles. The intermetallic FePt/PtBi core/shell nanoparticles can be obtained with the shortened Pt–Pt bond, which can greatly alleviate the adverse effect of the interlayer tensile strain effect induced by the large Bi atoms for ORR electrocatalysis. As a result, a 0.39 eV remission of oxygen adsorption was achieved compared to crude Pt (111) and a 10-times enhancement of specific activity than commercial Pt/C catalyst was obtained. Moreover, after 30,000 cycles, the mass activity retention of FePt@PtBi core/shell nanoparticles was as high as 82%, while those of PtFeBi and FePt nanoparticles were 36% and 37%, respectively. To this end, the indispensable role of biaxial and even multiaxial strain from different zone axis directions caused by the unique intermetallic nanocrystals is highly appealing for enhancing ORR electrocatalysis.

4.5. High-Entropy Alloys

Due to the ability to continuously adjust the surface electronic structure of alloy catalysts, high-entropy alloys have attracted increasing attention in electrocatalysis. This can break through the barrier where the adsorption energy of traditional alloys towards oxygen-containing intermediates cannot approach the vertex of the volcanic curve [191,192]. In particular, the core effects, including high-entropy, lattice distortion, sluggish diffusion and cocktail effect, also endow the high-entropy alloys with high structural stability, thus becoming kind of ideal candidate catalysts for ultradurable electrocatalysis [193]. Generally, the Sabatier theory has indicated that a desired catalyst should show the optimal bonding strength towards oxygen-containing intermediates, which has been widely reflected on various single metals or binary alloys [45,194,195]. Nevertheless, the traditional methods, including the *d*-band model and generalized coordination number model, etc., for associating adsorption energy cannot be extended to the complex high-entropy alloys [196,197]. To this end, Rossmeisl et al. developed a simple model to build the linear regression models via calculating the adsorption energies of *OH and *O on the IrPdPtRhRu (111) surface (Figure 11a,b) [198]. The ORR performance can be maximized through adjusting the whole compositions of high-entropy alloys, and the adsorption energies near to the apex of the volcano curve can be achieved on the optimized $Ir_{0.102}Pd_{0.320}Pt_{0.093}Rh_{0.196}Ru_{0.289}$. Afterwards, they further simplified the performance optimization of high-entropy alloys by

combining the dynamic simulations and DFT calculations with Bayesian optimization [199]. Therefore, the feasibility of high-entropy alloys in fuel cell-related electrocatalysis has been theoretically demonstrated by these studies.

However, high-entropy alloys are traditionally prepared through top-down methods, creating the bulk materials with very few active sites [200]. In order to make the high-entropy alloys meet the electrocatalysis, reducing the size is an inevitable trend to guarantee catalytic reaction occurrence. In light of the near-continuum distribution of the relevant adsorption energies, PtPdFeCoNi nanoparticles showed a positive-shifted ORR polarization curve compared with that of commercial Pt/C, with a positive half-wave potential of 0.920 V [201]. The lattice distortion effect and sluggish diffusion effect also endowed PtPdFeCoNi nanoparticles with a high mass activity of 1.23 A $mg_{Pt}{}^{-1}$ and specific activity of 1.80 mA cm^{-2}. This is not only superior to the commercial Pt/C, but also higher than that of low-entropy counterparts (PtCo nanoparticles). Furthermore, an anchoring-carbonization strategy was presented to embed Pt-based high-entropy alloys with sizes below 3 nm onto the pore walls of ordered mesoporous carbon (Figure 11c) [202]. The method was highly general and can be extended to the synthesis of a series of Pt-based ultrasmall high-entropy alloys, including senary PtFeCoNiCuZn, septenary PtRuIrFeCoNiCu, octonary PtRuIrFeCoNiCuZn and denary PtRuIrRhFeCoNiCuZnSn nanoparticles. As-prepared senary PtFeCoNiCuZn high-entropy alloy nanoparticles showed a higher ORR activity than those of low- and medium-entropy counterparts, demonstrating the enhanced electrocatalysis of high-entropy alloys (Figure 11d). In addition, such ultrasmall high-entropy alloys also exhibited a superior durability than that of commercial Pt/C catalysts, implying that the high-entropy alloys may be a promising model for ultradurable electrocatalysis.

Morphological regulation has been regarded as an efficient method to enhance ORR electrocatalysis, while the high-entropy alloys with anisotropic shapes are still difficult to synthesize in view of their harsh preparation conditions. Recently, several strategies have been presented to address this problem, such as the wet-chemical methods via introducing appropriate capping agents or strong reductants [203,204], the use of templates to control the anisotropic growth of multimetal nanocrystals [205] and the combination of auto-combustion and low-temperature reduction methods [206]. To obtain high-performance, high-entropy alloy-based ORR electrocatalysts, Guo, et al. used Ag nanowires as the templates to achieve the construction of ultrathin 2D high-entropy alloy subnanometer ribbons with a thickness of ~0.8 nm (Figure 12a,b) [207]. Several elements were uniformly distributed in the subnanometer ribbons, demonstrating the successfully formation of high-entropy alloys (Figure 12c). Note that this is the thinnest high-entropy alloy so far, and this method can be used to synthesize various high-entropy alloy subnanometer ribbons containing five to eight noble metal elements, such as senary PtPdIrRuAuAg, septenary PtPdIrRuAuRhAg and octonary HEA PtPdIrRuAuRhOsAg subnanometer ribbons. They demonstrated that the formation of high-entropy alloy subnanometer ribbons mainly involved the galvanic exchange pathway and co-reduction process during the wet-chemical synthesis, as well as the dealloying strategy realized the 2D structural evolution of the high-entropy alloy subnanometer ribbons (Figure 12d). In alkaline conditions, the ORR mass activity of the optimized quinary PtPdIrRuAg subnanometer ribbons was 21.0 times higher than that of commercial Pt/C (Figure 12e). After 10,000 potential cycles, there was almost no change in the ORR polarization curves of the PtPdIrRuAg, and over 30,000 potential cycles, the mass activities of PtPdIrRuAg were still as high as 2.42 A $mg_{Pt}{}^{-1}$ and 0.95 A $mg_{PGMs}{}^{-1}$, and their quinary high-entropy alloy phase and porous 2D structures can be well maintained (Figure 12f,g), confirming the advantages of high-entropy alloys with anisotropic structures.

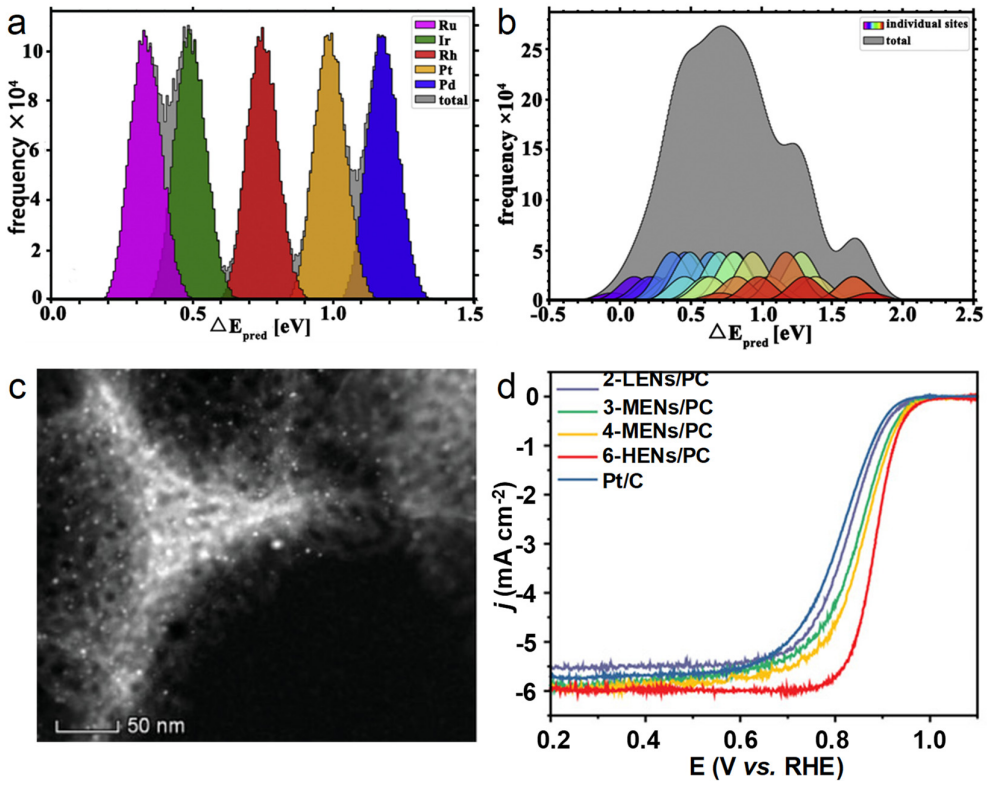

Figure 11. Enhancing ORR durability of Pt-based catalysts by high-entropy alloys. (**a**) Full span of predicted adsorption energies of (**a**) *OH and (**b**) *O based on DFT calculations (each color represents an individual binding site). Reprinted with permission from Ref. [198]. Copyright 2019 Elsevier. (**c**) Representative HAADF-STEM image of porous carbon-supported PtFeCoNiCuZn high-entropy alloy nanoparticles. (**d**) ORR polarization curves of porous carbon-supported PtFeCoNiCuZn high-entropy alloy nanoparticles and the medium- and low-entropy counterparts and commercial Pt/C catalysts. Reprinted with permission from Ref. [202]. Copyright 2022 Wiley.

It has been found that the electrocatalytic behavior can be affected by the atomic ordering structures, which has been further extended into high-entropy alloy systems. Combining the advantages of high-entropy and ordered intermetallic structures, high-entropy intermetallics have been presented to serve as highly stable catalysts for ORR electrocatalysis [187,208]. However, the formation of high-entropy intermetallics not only needs to overcome the mutual solubility of various elements, but also needs to cross the energy barrier of disorder-to-order phase transition, challenging more severe synthesis problems of high-entropy intermetallics. In order to overcome this difficulty, Xia's group added the carbon supports into a prereaction solution to avoid the agglomeration of nanoparticles under the very high annealing temperature environment [167]. After annealing at 850 °C, (PtIr)(FeCoCu) high-entropy intermetallic nanoparticles with an average diameter of 6 nm and a uniform distribution were directly synthesized with a similar phase structure as $L1_0$-PtFe intermetallics. The significantly enhanced activity and durability were reflected on the (PtIr)(FeCoCu) high-entropy intermetallic nanoparticles, revealing the advantages of the combination of high-entropies and intermetallic structures.

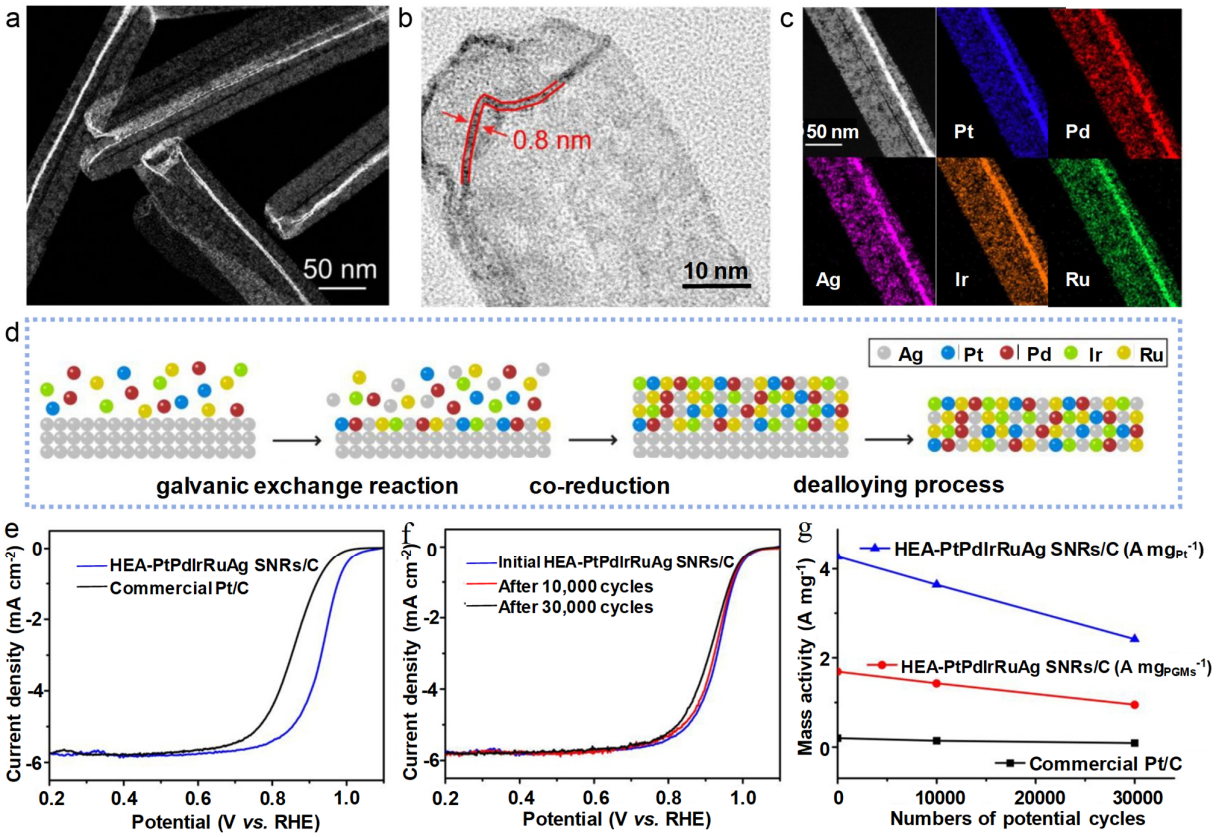

Figure 12. Enhancing ORR durability of Pt-based catalysts by high-entropy alloys with anisotropic morphologies. Representative (**a**) HAADF-STEM and (**b**) high-magnification TEM images of PtPdIrRuAg high-entropy alloy subnanometer ribbons. (**c**) STEM-elemental mappings of PtPdIrRuAg high-entropy alloy subnanometer ribbons. (**d**) Schematic illustration for the formation mechanism of PtPdIrRuAg high-entropy alloy subnanometer ribbons. (**e**) ORR polarization curves of PtPdIrRuAg high-entropy alloy subnanometer ribbons and commercial Pt/C catalysts. (**f**) ORR polarization curves of PtPdIrRuAg high-entropy alloy subnanometer ribbons before and after different potential cycles. (**g**) The mass activities of PtPdIrRuAg high-entropy alloy subnanometer ribbons and commercial Pt/C catalysts before and after different potential cycles. Reprinted with permission from Ref. [207]. Copyright 2022 ACS.

4.6. Others

Beyond the above interesting structural designs, there are still several special strategies to further improve the ORR durability. The basic principle of these strategies is to maintain/improve activity while enhancing durability. Similarly, inhibiting the loss of active metal and improving the structural stability are the dominant reason for the enhancement of durability. For example, the heterostructure represents a new idea to adjust the adsorption capacity towards intermediates and achieve a high structural stability [209–211]. Such a heterostructure involves the metal/metal, metal/compounds and metal/supports interfaces. For this purpose, Yin et al. constructed PtCo–PtSn heterostructural nanoparticles to achieve ultradurable electrocatalysis [212]. Specifically, the ORR activity of the optimized PtCo–PtSn nanoparticles was 1158 mA mg_{Pt}^{-1}, and after 30,000 cycles, the activity degradation was only 27.4%. The charge redistribution caused by the construction of heterointerface adjusted the electronic structures of Pt, thus the *d*-band center was reduced to −2.45 eV. The strong interaction between PtCo and PtSn efficiently inhibited the separation of two phases and limited the leaching of nonprecious metals. Additionally, the Ostwald ripening and Pt migration were also weakened, thereby boosting ORR durability. In addition to the interface engineering, surface engineering, strain effect and atomic arrangement engineering are also effective methods to achieve ultradurable ORR electrocatalysis.

5. Conclusions

The performance of fuel cells is highly dependent on the ORR catalysts. Although the alloying strategy has well addressed the low activity issues of Pt metals, the poor durability still exists due to the corrosion of carbon supports, the preferential leaching of active metal elements, the instability of surface low-coordinated atoms and the sintering/agglomeration of nanocrystals. Recently, the advanced structural regulation strategies have witnessed the development of ultradurable ORR catalysts. In this review, the operation mechanism of ORR electrocatalysis and limitation of traditional Pt-based catalysts are first discussed, and then several important structural designs for ultradurable ORR catalysts are summarized from the following aspects: the optimization of supports, heteroatom-doped alloys, core/shell structures, intermetallics, high-entropy alloys and others. In particular, the structure–performance relationship between these unique advanced structures and ultradurability is emphatically concerned. Although the significant achievements in this field have been made in recent years, several existing obstacles and issues are still expected to be addressed.

(1) Developing new support materials to strengthen the interaction between active metals and supports. The corrosion of carbon is still the dominant reason why most catalysts cannot be reproduced in practical fuel cells, especially at such a large current. Although some strategies have been developed to improve the stability of traditional support materials, it is still difficult to meet the needs of long-term operation. Therefore, the development of new corrosion-resistant supports may provide an insightful scientific basis for the further commercialization of fuel cells in the future.

(2) Developing the new catalyst systems to further eliminate the effect of poor durability of Pt-based catalysts. Although a large number of strategies have been reported to address the poor durability of Pt-based catalysts during the long-term ORR cycles, the influencing factors have not been thoroughly eliminated. For example, despite the loss of alloying metals in the ORR process which can be effectively reduced by the doping of a third metal, there will still be a leaching phenomenon, which still decreases the durability. Therefore, the development of new routes to further improve durability, especially focusing on the combination of reported strategies, will be necessary in the future.

(3) Establishing the relationship between the catalysts structure and ORR durability through in situ and ex situ characterizations. The rapid development of (sub)-nanomaterials has stimulated the requirement of more advanced characterizations. In terms of ultradurable Pt-based ORR catalysts, it is important to characterize the structure more accurately. Particularly, it is meaningful to reveal the structural evolution of the catalysts during the long-term ORR tests through in situ or ex situ characterizations. For example, using in situ synchrotron radiation technologies to reveal the change of metal bond length in Pt-based catalysts during ORR processes may help us to better understand the essence of catalyst durability enhancement. These advanced characterization techniques may guide us to design more effective catalysts.

(4) The application of ultradurable Pt-based catalysts in practical fuel cells. Most of catalysts have shown excellent catalytic performance under the condition of half-cell, but they are rarely used in practical fuel cells. This is mainly due to the fact that the harsh operating environment of proton exchange membrane fuel cells makes Pt-based catalysts more unstable. Therefore, it is very important to explore the attenuation behavior of these ultradurable catalysts in practical fuel cells and develop catalysts suitable for long-term durability and practical fuel cells. In addition, the decay behavior of catalysts under working conditions may be different from that under half-cell conditions, so understanding the evolution of catalyst structure under working conditions will also be a research trend in this field in the future.

In summary, it has been shown that the designs of ultradurable ORR catalysts have clearly contributed to the fast development of PEMFCs, and it has been believed that this is a research frontier in the material science community and will open up new possibilities

to obtain more efficient catalysts for advanced energy conversion devices in terms of long-term operation conditions.

Author Contributions: Conceptualization and writing—original draft preparation, Z.L.; software, P.Z.; validation, Y.Z.; formal analysis, W.J.; visualization, B.Z.; supervision, funding acquisition and resources, X.C.; conceptualization, funding acquisition and writing—review and editing, M.L. All authors have read and agreed to the published version of the manuscript.

Funding: This study was financially supported by the National Natural Science Foundation of China (Nos. 21905146 and 52303361), the Natural Science Foundation of Heilongjiang Province of China (No. LH2023B025), the University Nursing Program for Young Scholars with Creative Talents of Heilongjiang Province of China (No. UNPYSCT-2020066), the Heilongjiang Provincial Key Laboratory of Surface Active Agent and Auxiliary (No. BMHXJKF008), the Qiqihar University Graduate Innovation Foundation of China (No. YJSCX2022011), the Natural Science Fundamental Research Project of Department of Education of Heilongjiang Province of China (No. 145309203) and the China Postdoctoral Science Foundation (No. 2022M710201).

Data Availability Statement: No new data was created or analyzed in this study. Data sharing is not applicable to this article.

Conflicts of Interest: The authors declare no conflict of interest.

References

1. Lewis, N.S. Research Opportunities to Advance Solar Energy Utilization. *Science* **2016**, *351*, aad1920. [CrossRef] [PubMed]
2. Jiao, K.; Xuan, J.; Du, Q.; Bao, Z.; Xie, B.; Wang, B.; Zhao, Y.; Fan, L.; Wang, H.; Hou, Z.; et al. Designing the Next Generation of Proton-Exchange Membrane Fuel Cells. *Nature* **2021**, *595*, 361–369. [CrossRef] [PubMed]
3. Zhang, S.; Tan, H.; Rui, X.; Yu, Y. Vanadium-Based Materials: Next Generation Electrodes Powering the Battery Revolution? *Acc. Chem. Res.* **2020**, *53*, 1660–1671. [CrossRef] [PubMed]
4. Li, M.; Wang, J.; Guo, X.; Li, J.; Huang, Y.; Geng, S.; Yu, Y.; Liu, Y.; Yang, W. Structural Engineering of Fe-Doped Ni_2P Nanosheets Arrays for Enhancing Bifunctional Electrocatalysis towards Overall Water Splitting. *Appl. Surf. Sci.* **2021**, *536*, 147909. [CrossRef]
5. Gu, Y.; Xi, B.; Wei, R.; Fu, Q.; Qain, Y.; Xiong, S. Sponge Assembled by Graphene Nanocages with Double Active Sites to Accelerate Alkaline HER Kinetics. *Nano Lett.* **2020**, *20*, 8375–8383. [CrossRef]
6. Yang, W.; Wang, Z.; Zhang, W.; Guo, S. Electronic-Structure Tuning of Water-Splitting Nanocatalysts. *Trends Chem.* **2019**, *1*, 259–271. [CrossRef]
7. Li, L.; Tian, F.; Qiu, L.; Wu, F.; Yang, W.; Yu, Y. Recent Progress on Ruthenium-Based Electrocatalysts towards the Hydrogen Evolution Reaction. *Catalysts* **2023**, *13*, 1497. [CrossRef]
8. Shao, M.; Chang, Q.; Dodelet, J.-P.; Chenitz, R. Recent Advances in Electrocatalysts for Oxygen Reduction Reaction. *Chem. Rev.* **2016**, *116*, 3594–3657. [CrossRef]
9. Cullen, D.A.; Neyerlin, K.C.; Ahluwalia, R.K.; Mukundan, R.; More, K.L.; Borup, R.L.; Weber, A.Z.; Myers, D.J.; Kusoglu, A. New Roads and Challenges for Fuel Cells in Heavy-Duty Transportation. *Nat. Energy* **2021**, *6*, 462–474. [CrossRef]
10. Kim, J.; Hong, Y.; Lee, K.; Kim, J.Y. Highly Stable Pt-Based Ternary Systems for Oxygen Reduction Reaction in Acidic Electrolytes. *Adv. Energy Mater.* **2020**, *10*, 2002049. [CrossRef]
11. Zhang, Q.; Dong, S.; Shao, P.; Zhu, Y.; Mu, Z.; Sheng, D.; Zhang, T.; Jiang, X.; Shao, R.; Ren, Z.; et al. Covalent Organic Framework–Based Porous Ionomers for High-Performance Fuel Cells. *Science* **2022**, *378*, 181–186. [CrossRef] [PubMed]
12. Ma, S.-Y.; Ma, T.; Hu, Q.; Yang, H.-P.; He, C.-X. Ternary PtRuTe Alloy Nanofibers as an Efficient and Durable Electrocatalyst for Hydrogen Oxidation Reaction in Alkaline Media. *Sci. China Mater.* **2022**, *65*, 3462–3469. [CrossRef]
13. Su, L.; Jin, Y.; Fan, X.; Liu, Z.; Luo, W. pH-Dependent Binding Energy-Induced Inflection-Point Behaviors for pH-Universal Hydrogen Oxidation Reaction. *Sci. China Chem.* **2023**, *66*, 3262–3268. [CrossRef]
14. Wang, X.; Zhao, L.; Li, X.; Liu, Y.; Wang, Y.; Yao, Q.; Xie, J.; Xue, Q.; Yan, Z.; Yuan, X.; et al. Atomic-Precision Pt_6 Nanoclusters for Enhanced Hydrogen Electro-Oxidation. *Nat. Commun.* **2022**, *13*, 1596. [CrossRef]
15. Yuan, S.; Zhang, J.; Hu, L.; Li, J.; Li, S.; Gao, Y.; Zhang, Q.; Gu, L.; Yang, W.; Feng, X.; et al. Decarboxylation-Induced Defects in MOF-Derived Single Cobalt Atom@Carbon Electrocatalysts for Efficient Oxygen Reduction. *Angew. Chem. Int. Ed.* **2021**, *60*, 21685–21690. [CrossRef]
16. Li, M.; Tian, F.; Lin, T.; Tao, L.; Guo, X.; Chao, Y.; Guo, Z.; Zhang, Q.; Gu, L.; Yang, W.; et al. High-Index Faceted PdPtCu Ultrathin Nanorings Enable Highly Active and Stable Oxygen Reduction Electrocatalysis. *Small Methods* **2021**, *5*, 2100154. [CrossRef]
17. Zhao, Z.; Chen, C.; Liu, Z.; Huang, J.; Wu, M.; Liu, H.; Li, Y.; Huang, Y. Pt-Based Nanocrystal for Electrocatalytic Oxygen Reduction. *Adv. Mater.* **2019**, *31*, 1808115. [CrossRef]
18. Zhang, J.; Zhang, J.; He, F.; Chen, Y.; Zhu, J.; Wang, D.; Mu, S.; Yang, H.Y. Defect and Doping Co-Engineered Non-Metal Nanocarbon ORR Electrocatalyst. *Nano-Micro Lett.* **2021**, *13*, 65. [CrossRef]

19. Kodama, K.; Nagai, T.; Kuwaki, A.; Jinnouchi, R.; Morimoto, Y. Challenges in Applying Highly Active Pt-Based Nanostructured Catalysts for Oxygen Reduction Reactions to Fuel Cell Vehicles. *Nat. Nanotechnol.* **2021**, *16*, 140–147. [CrossRef]
20. Nie, Y.; Li, L.; Wei, Z. Recent Advancements in Pt and Pt-Free Catalysts for Oxygen Reduction Reaction. *Chem. Soc. Rev.* **2015**, *44*, 2168–2201. [CrossRef]
21. Zhang, X.; Li, H.; Yang, J.; Lei, Y.; Wang, C.; Wang, J.; Tang, Y.; Mao, Z. Recent Advances in Pt-Based Electrocatalysts for PEMFCs. *RSC Adv.* **2021**, *11*, 13316–13328. [CrossRef] [PubMed]
22. Ahn, C.-Y.; Park, J.E.; Kim, S.; Kim, O.-H.; Hwang, W.; Her, M.; Kang, S.Y.; Park, S.; Kwon, O.J.; Park, H.S.; et al. Differences in the Electrochemical Performance of Pt-Based Catalysts Used for Polymer Electrolyte Membrane Fuel Cells in Liquid Half- and Full-Cells. *Chem. Rev.* **2021**, *121*, 15075–15140. [CrossRef] [PubMed]
23. Cao, S.; Sun, T.; Li, J.-R.; Li, Q.-Z.; Hou, C.-C.; Sun, Q. The Cathode Catalysts of Hydrogen Fuel Cell: From Laboratory toward Practical Application. *Nano Res.* **2023**, *16*, 4365–4380. [CrossRef]
24. Luo, M.; Koper, M.T.M. A Kinetic Descriptor for the Electrolyte Effect on the Oxygen Reduction Kinetics on Pt (111). *Nat. Catal.* **2022**, *5*, 615–623. [CrossRef]
25. Zaman, S.; Huang, L.; Douka, A.I.; Yang, H.; You, B.; Xia, B.Y. Oxygen Reduction Electrocatalysts toward Practical Fuel Cells: Progress and Perspectives. *Angew. Chem. Int. Ed.* **2021**, *60*, 17832–17852. [CrossRef] [PubMed]
26. Wang, Y.; Wang, L.; Fu, H. Research Progress of Fe-N-C Catalysts for the Electrocatalytic Oxygen Reduction Reaction. *Sci. China Mater.* **2022**, *65*, 1701–1722. [CrossRef]
27. Wu, X.; Xie, W.; Liu, X.; Liu, X.; Zhao, Q. Two-Dimensional Fe-N-C Nanosheets for Efficient Oxygen Reduction Reaction. *Catalysts* **2022**, *12*, 1276. [CrossRef]
28. Liu, Y.; Liu, X.; Lv, Z.; Liu, R.; Li, L.; Wang, J.; Yang, W.; Jiang, X.; Feng, X.; Wang, B. Tuning the Spin State of the Iron Center by Bridge-Bonded Fe-O-Ti Ligands for Enhanced Oxygen Reduction. *Angew. Chem. Int. Ed.* **2022**, *61*, e202117617. [CrossRef]
29. Gu, Y.; Xi, B.J.; Zhang, H.; Ma, Y.C.; Xiong, S.L. Activation of Main-Group Antimony Atomic Sites for Oxygen Reduction Catalysis. *Angew. Chem. Int. Ed.* **2022**, *61*, e202202200. [CrossRef]
30. Ma, Z.; Cano, Z.P.; Yu, A.; Chen, Z.; Jiang, G.; Fu, X.; Yang, L.; Wu, T.; Bai, Z.; Lu, J. Enhancing Oxygen Reduction Activity of Pt-Based Electrocatalysts: From Theoretical Mechanisms to Practical Methods. *Angew. Chem. Int. Ed.* **2020**, *59*, 18334–18348. [CrossRef]
31. Sapkota, P.; Lim, S.; Aguey-Zinsou, K.-F. Superior Performance of an Iron-Platinum/Vulcan Carbon Fuel Cell Catalyst. *Catalysts* **2022**, *12*, 1369. [CrossRef]
32. Hou, B.; Luo, X.; Zheng, Z.; Tang, R.; Zhang, Q.; Gholizadeh, M.; Wang, C.; Tan, Z. An Efficient Electrocatalyst (PtCo/C) for the Oxygen Reduction Reaction. *Catalysts* **2022**, *12*, 794. [CrossRef]
33. Huang, L.; Su, Y.-Q.; Qi, R.; Dang, D.; Qin, Y.; Xi, S.; Zaman, S.; You, B.; Ding, S.; Xia, B.Y. Boosting Oxygen Reduction via Integrated Construction and Synergistic Catalysis of Porous Platinum Alloy and Defective Graphitic Carbon. *Angew. Chem. Int. Ed.* **2021**, *60*, 25530–25537. [CrossRef] [PubMed]
34. Yang, C.; Gao, Y.; Ma, T.; Bai, M.; He, C.; Ren, X.; Luo, X.; Wu, C.; Li, S.; Cheng, C. Metal Alloys-Structured Electrocatalysts: Metal-Metal Interactions, Coordination Microenvironments, and Structural Property-Reactivity Relationships. *Adv. Mater.* **2023**, *35*, 2301836. [CrossRef]
35. Kim, D.-G.; Sohn, Y.; Jang, I.; Yoo, S.J.; Kim, P. Formation Mechanism of Carbon-Supported Hollow PtNi Nanoparticles via One-Step Preparations for Use in the Oxygen Reduction Reaction. *Catalysts* **2022**, *12*, 513. [CrossRef]
36. Li, C.; Huang, B.; Luo, M.; Qin, Y.; Sun, Y.; Li, Y.; Yang, Y.; Wu, D.; Li, M.; Guo, S. An Efficient Ultrathin PtFeNi Nanowire/Ionic Liquid Conjugate Electrocatalyst. *Appl. Catal. B* **2019**, *256*, 117828. [CrossRef]
37. Yoshida, T.; Kojima, K. Toyota MIRAI Fuel Cell Vehicle and Progress toward a Future Hydrogen Society. *Electrochem. Soc. Interface* **2015**, *24*, 45. [CrossRef]
38. Borup, R.L.; Kusoglu, A.; Neyerlin, K.C.; Mukundan, R.; Ahluwalia, R.K.; Cullen, D.A.; More, K.L.; Weber, A.Z.; Myers, D.J. Recent Developments in Catalyst-Related PEM Fuel Cell Durability. *Curr. Opin. Electrochem.* **2020**, *21*, 192–200. [CrossRef]
39. Gao, L.; Li, X.; Yao, Z.; Bai, H.; Lu, Y.; Ma, C.; Lu, S.; Peng, Z.; Yang, J.; Pan, A.; et al. Unconventional *p-d* Hybridization Interaction in PtGa Ultrathin Nanowires Boosts Oxygen Reduction Electrocatalysis. *J. Am. Chem. Soc.* **2019**, *141*, 18083–18090. [CrossRef]
40. Li, K.; Li, X.; Huang, H.; Luo, L.; Li, X.; Yan, X.; Ma, C.; Si, R.; Yang, J.; Zeng, J. One-Nanometer-Thick PtNiRh Trimetallic Nanowires with Enhanced Oxygen Reduction Electrocatalysis in Acid Media: Integrating Multiple Advantages into One Catalyst. *J. Am. Chem. Soc.* **2018**, *140*, 16159–16167. [CrossRef]
41. Wei, M.; Huang, L.; Li, L.; Ai, F.; Su, J.; Wang, J. Coordinatively Unsaturated PtCo Flowers Assembled with Ultrathin Nanosheets for Enhanced Oxygen Reduction. *ACS Catal.* **2022**, *12*, 6478–6485. [CrossRef]
42. Zhu, X.; Huang, L.; Wei, M.; Tsiakaras, P.; Shen, P.K. Highly Stable Pt-Co Nanodendrite in Nanoframe with Pt Skin Structured Catalyst for Oxygen Reduction Electrocatalysis. *Appl. Catal. B* **2021**, *281*, 119460. [CrossRef]
43. Tian, X.; Zhao, X.; Su, Y.-Q.; Wang, L.; Wang, H.; Dang, D.; Chi, B.; Liu, H.; Hensen, E.J.M.; Lou, X.W.; et al. Engineering Bunched Pt-Ni Alloy Nanocages for Efficient Oxygen Reduction in Practical Fuel Cells. *Science* **2019**, *366*, 850–856. [CrossRef] [PubMed]
44. Zheng, Y.; Petersen, A.S.; Wan, H.; Hübner, R.; Zhang, J.; Wang, J.; Qi, H.; Ye, Y.; Liang, C.; Yang, J.; et al. Scalable and Controllable Synthesis of Pt-Ni Bunched-Nanocages Aerogels as Efficient Electrocatalysts for Oxygen Reduction Reaction. *Adv. Energy Mater.* **2023**, *13*, 2204257. [CrossRef]

45. Luo, M.; Qin, Y.; Li, M.; Sun, Y.; Li, C.; Li, Y.; Yang, Y.; Lv, F.; Wu, D.; Zhou, P.; et al. Interface Modulation of Twinned PtFe Nanoplates Branched 3D Architecture for Oxygen Reduction Catalysis. *Sci. Bull.* **2020**, *65*, 97–104. [CrossRef]
46. Zhu, R.; Yu, R.; Yin, K.; Zhang, S.; Chung-Yen Jung, J.; Zhao, Y.; Li, M.; Xia, Z.; Zhang, J. Integration of Multiple Advantages into One Catalyst: Non-CO Pathway of Methanol Oxidation Electrocatalysis on Surface Ir-Modulated PtFeIr Jagged Nanowires. *J. Colloid Interface Sci.* **2023**, *640*, 348–358. [CrossRef]
47. Shi, Y.; Lyu, Z.; Zhao, M.; Chen, R.; Nguyen, Q.N.; Xia, Y. Noble-Metal Nanocrystals with Controlled Shapes for Catalytic and Electrocatalytic Applications. *Chem. Rev.* **2021**, *121*, 649–735. [CrossRef]
48. Zhang, S.; Ling, F.; Wang, L.; Xu, R.; Ma, M.; Cheng, X.; Bai, R.; Shao, Y.; Huang, H.; Li, D.; et al. An Open-Ended Ni_3S_2-Co_9S_8 Heterostructures Nanocage Anode with Enhanced Reaction Kinetics for Superior Potassium-Ion Batteries. *Adv. Mater.* **2022**, *34*, 2201420. [CrossRef]
49. Li, M.; Xia, Z.; Luo, M.; He, L.; Tao, L.; Yang, W.; Yu, Y.; Guo, S. Structural Regulation of Pd-Based Nanoalloys for Advanced Electrocatalysis. *Small Sci.* **2021**, *1*, 2100061. [CrossRef]
50. Cheng, H.; Gui, R.; Liu, S.; Xie, Y.; Wu, C. Local Structure Engineering for Active Sites in Fuel Cell Electrocatalysts. *Sci. China Chem.* **2020**, *63*, 1543–1556. [CrossRef]
51. Qin, Y.; Zhang, W.; Guo, K.; Liu, X.; Liu, J.; Liang, X.; Wang, X.; Gao, D.; Gan, L.; Zhu, Y.; et al. Fine-Tuning Intrinsic Strain in Penta-Twinned Pt-Cu-Mn Nanoframes Boosts Oxygen Reduction Catalysis. *Adv. Funct. Mater.* **2020**, *30*, 1910107. [CrossRef]
52. Guo, N.; Xue, H.; Bao, A.; Wang, Z.; Sun, J.; Song, T.; Ge, X.; Zhang, W.; Huang, K.; He, F.; et al. Achieving Superior Electrocatalytic Performance by Surface Copper Vacancy Defects during Electrochemical Etching Process. *Angew. Chem. Int. Ed.* **2020**, *59*, 13778–13784. [CrossRef] [PubMed]
53. Takimoto, D.; Toma, S.; Suda, Y.; Shirokura, T.; Tokura, Y.; Fukuda, K.; Matsumoto, M.; Imai, H.; Sugimoto, W. Platinum Nanosheets Synthesized via Topotactic Reduction of Single-Layer Platinum Oxide Nanosheets for Electrocatalysis. *Nat. Commun.* **2023**, *14*, 19. [CrossRef] [PubMed]
54. Jiang, Y.; Yang, K.; Li, M.; Xu, D.; Ma, Z. Engineering the Spin Configuration of Electrocatalysts for Electrochemical Renewable Conversions. *Mater. Chem. Front.* **2024**. [CrossRef]
55. Zhang, J.; Yuan, Y.; Gao, L.; Zeng, G.; Li, M.; Huang, H. Stabilizing Pt-Based Electrocatalysts for Oxygen Reduction Reaction: Fundamental Understanding and Design Strategies. *Adv. Mater.* **2021**, *33*, 2006494. [CrossRef] [PubMed]
56. Zaman, S.; Chen, S. A Perspective on Inaccurate Measurements in Oxygen Reduction and Carbon Dioxide Reduction Reactions. *J. Catal.* **2023**, *421*, 221–227. [CrossRef]
57. Fan, J.; Chen, M.; Zhao, Z.; Zhang, Z.; Ye, S.; Xu, S.; Wang, H.; Li, H. Bridging the Gap between Highly Active Oxygen Reduction Reaction Catalysts and Effective Catalyst Layers for Proton Exchange Membrane Fuel Cells. *Nat. Energy* **2021**, *6*, 475–486. [CrossRef]
58. Zaman, S.; Tian, X.; Xia, B.Y. Bridging Oxygen Reduction Performance Gaps in Half and Full Cells: Challenges and Perspectives. *Mater. Chem. Front.* **2023**, *7*, 4605–4612. [CrossRef]
59. Lei, W.; Li, M.; He, L.; Meng, X.; Mu, Z.; Yu, Y.; Ross, F.M.; Yang, W. A General Strategy for Bimetallic Pt-Based Nano-Branched Structures as Highly Active and Stable Oxygen Reduction and Methanol Oxidation Bifunctional Catalysts. *Nano Res.* **2020**, *13*, 638–645. [CrossRef]
60. Stamenkovic, V.R.; Fowler, B.; Mun, B.S.; Wang, G.; Ross, P.N.; Lucas, C.A.; Marković, N.M. Improved Oxygen Reduction Activity on $Pt_3Ni(111)$ via Increased Surface Site Availability. *Science* **2007**, *315*, 493–497. [CrossRef]
61. Tao, L.; Xia, Z.; Zhang, Q.; Sun, Y.; Li, M.; Yin, K.; Gu, L.; Guo, S. Spiny Pd/PtFe Core/Shell Nanotubes with Rich High-Index Facets for Efficient Electrocatalysis. *Sci. Bull.* **2021**, *66*, 44–51. [CrossRef] [PubMed]
62. Iqbal, M.; Bando, Y.; Sun, Z.; Wu, K.C.W.; Rowan, A.E.; Na, J.; Guan, B.Y.; Yamauchi, Y. In Search of Excellence: Convex *versus* Concave Noble Metal Nanostructures for Electrocatalytic Applications. *Adv. Mater.* **2021**, *33*, 2004554. [CrossRef] [PubMed]
63. Xiao, C.; Lu, B.-A.; Xue, P.; Tian, N.; Zhou, Z.-Y.; Lin, X.; Lin, W.-F.; Sun, S.-G. High-Index-Facet- and High-Surface-Energy Nanocrystals of Metals and Metal Oxides as Highly Efficient Catalysts. *Joule* **2020**, *4*, 2562–2598. [CrossRef]
64. Ioroi, T.; Siroma, Z.; Yamazaki, S.-I.; Yasuda, K. Electrocatalysts for PEM Fuel Cells. *Adv. Energy Mater.* **2019**, *9*, 1801284. [CrossRef]
65. Alekseenko, A.; Pavlets, A.; Moguchikh, E.; Tolstunov, M.; Gribov, E.; Belenov, S.; Guterman, V. Platinum-Containing Nanoparticles on N-Doped Carbon Supports as an Advanced Electrocatalyst for the Oxygen Reduction Reaction. *Catalysts* **2022**, *12*, 414. [CrossRef]
66. Castanheira, L.; Dubau, L.; Mermoux, M.; Berthomé, G.; Caqué, N.; Rossinot, E.; Chatenet, M.; Maillard, F. Carbon Corrosion in Proton-Exchange Membrane Fuel Cells: From Model Experiments to Real-Life Operation in Membrane Electrode Assemblies. *ACS Catal.* **2014**, *4*, 2258–2267. [CrossRef]
67. Zhu, S.; Yang, L.; Bai, J.; Chu, Y.; Liu, J.; Jin, Z.; Liu, C.; Ge, J.; Xing, W. Ultra-Stable Pt_5La Intermetallic Compound towards Highly Efficient Oxygen Reduction Reaction. *Nano Res.* **2023**, *16*, 2035–2040. [CrossRef]
68. Liu, B.; Feng, R.; Busch, M.; Wang, S.; Wu, H.; Liu, P.; Gu, J.; Bahadoran, A.; Matsumura, D.; Tsuji, T.; et al. Synergistic Hybrid Electrocatalysts of Platinum Alloy and Single-Atom Platinum for an Efficient and Durable Oxygen Reduction Reaction. *ACS Nano* **2022**, *16*, 14121–14133. [CrossRef]
69. Xiao, F.; Wang, Q.; Xu, G.-L.; Qin, X.; Hwang, I.; Sun, C.-J.; Liu, M.; Hua, W.; Wu, H.-W.; Zhu, S.; et al. Atomically Dispersed Pt and Fe Sites and Pt-Fe Nanoparticles for Durable Proton Exchange Membrane Fuel Cells. *Nat. Catal.* **2022**, *5*, 503–512. [CrossRef]

70. Cheng, Q.; Yang, S.; Fu, C.; Zou, L.; Zou, Z.; Jiang, Z.; Zhang, J.; Yang, H. High-Loaded Sub-6 nm Pt_1Co_1 Intermetallic Compounds with Highly Efficient Performance Expression in PEMFCs. *Energy Environ. Sci.* **2022**, *15*, 278–286. [CrossRef]
71. Liang, J.; Li, N.; Zhao, Z.; Ma, L.; Wang, X.; Li, S.; Liu, X.; Wang, T.; Du, Y.; Lu, G.; et al. Tungsten-Doped $L1_0$-PtCo Ultrasmall Nanoparticles as a High-Performance Fuel Cell Cathode. *Angew. Chem. Int. Ed.* **2019**, *58*, 15471–15477. [CrossRef] [PubMed]
72. Xia, W.; Mahmood, A.; Liang, Z.; Zou, R.; Guo, S. Earth-Abundant Nanomaterials for Oxygen Reduction. *Angew. Chem. Int. Ed.* **2016**, *55*, 2650–2676. [CrossRef] [PubMed]
73. Hou, J.; Yang, M.; Ke, C.; Wei, G.; Priest, C.; Qiao, Z.; Wu, G.; Zhang, J. Platinum-Group-Metal Catalysts for Proton Exchange Membrane Fuel Cells: From Catalyst Design to Electrode Structure Optimization. *EnergyChem* **2020**, *2*, 100023. [CrossRef]
74. Guo, S.; Zhang, S.; Sun, S. Tuning Nanoparticle Catalysis for the Oxygen Reduction Reaction. *Angew. Chem. Int. Ed.* **2013**, *52*, 8526–8544. [CrossRef]
75. Wang, X.; Li, Z.; Qu, Y.; Yuan, T.; Wang, W.; Wu, Y.; Li, Y. Review of Metal Catalysts for Oxygen Reduction Reaction: From Nanoscale Engineering to Atomic Design. *Chem* **2019**, *5*, 1486–1511. [CrossRef]
76. Nørskov, J.K.; Rossmeisl, J.; Logadottir, A.; Lindqvist, L.; Kitchin, J.R.; Bligaard, T.; Jónsson, H. Origin of the Overpotential for Oxygen Reduction at a Fuel-Cell Cathode. *J. Phys. Chem. B* **2004**, *108*, 17886–17892. [CrossRef]
77. Stamenkovic, V.; Mun, B.S.; Mayrhofer, K.J.J.; Ross, P.N.N.; Markovic, N.M.; Rossmeisl, J.; Greeley, J.; Nørskov, J.K. Changing the Activity of Electrocatalysts for Oxygen Reduction by Tuning the Surface Electronic Structure. *Angew. Chem. Int. Ed.* **2006**, *45*, 2897–2901. [CrossRef] [PubMed]
78. Alfaro-López, H.M.; Valdés-Madrigal, M.A.; Rojas-Chávez, H.; Cruz-Martínez, H.; Padilla-Islas, M.A.; Tellez-Cruz, M.M.; Solorza-Feria, O. A Trimetallic Pt_2NiCo/C Electrocatalyst with Enhanced Activity and Durability for Oxygen Reduction Reaction. *Catalysts* **2020**, *10*, 170. [CrossRef]
79. Liu, Z.; Zhao, Z.; Peng, B.; Duan, X.; Huang, Y. Beyond Extended Surfaces: Understanding the Oxygen Reduction Reaction on Nanocatalysts. *J. Am. Chem. Soc.* **2020**, *142*, 17812–17827. [CrossRef]
80. Sun, Y.; Tian, J.; Mu, Z.; Tian, B.; Zhou, Q.; Liu, C.; Liu, S.; Wu, Q.; Ding, M. Unravelling the Critical Role of Surface Nafion Adsorption in Pt-Catalyzed Oxygen Reduction Reaction by in situ Electrical Transport Spectroscopy. *Sci. China Chem.* **2022**, *65*, 2290–2298. [CrossRef]
81. Maillard, F.; Silva, W.O.; Castanheira, L.; Dubau, L.; Lima, F.H.B. Carbon Corrosion in Proton-Exchange Membrane Fuel Cells: Spectrometric Evidence for Pt-Catalysed Decarboxylation at Anode-Relevant Potentials. *ChemPhysChem* **2019**, *20*, 3106–3111. [CrossRef] [PubMed]
82. Ortíz-Herrera, J.C.; Tellez-Cruz, M.M.; Solorza-Feria, O.; Medina, D.I. Effect of Different Carbon Supports on the Activity of PtNi Bimetallic Catalysts toward the Oxygen Reduction. *Catalysts* **2022**, *12*, 477. [CrossRef]
83. Li, C.; Clament Sagaya Selvam, N.; Fang, J. Shape-Controlled Synthesis of Platinum-Based Nanocrystals and Their Electrocatalytic Applications in Fuel Cells. *Nano Micro Lett.* **2023**, *15*, 83. [CrossRef]
84. Nakaya, Y.; Furukawa, S. Catalysis of Alloys: Classification, Principles, and Design for a Variety of Materials and Reactions. *Chem. Rev.* **2023**, *123*, 5859–5947. [CrossRef]
85. Wang, X.; Li, J.; Yang, X.; Zhao, F.; Li, Y.; Zhang, D.; Gan, L.-Y.; Yao, K.X.; Yuan, Q. Low-Coordinated Surface Sites Make Truncated Pd Tetrahedrons as Robust ORR Electrocatalysts Outperforming Pt for DMFC Devices. *Nano Res.* **2022**, *15*, 7951–7958. [CrossRef]
86. Liu, B.; Yang, H.; Hu, P.; Wang, G.-S.; Guo, Y.; Zhao, H. Dimension Engineering in Noble-Metal-Based Nanocatalysts. *Catalysts* **2024**, *14*, 9. [CrossRef]
87. Parthasarathy, P.; Virkar, A.V. Electrochemical Ostwald Ripening of Pt and Ag Catalysts Supported on Carbon. *J. Power Sources* **2013**, *234*, 82–90. [CrossRef]
88. Chen, Y.; Cheng, T.; Goddard, W.A., III. Atomistic Explanation of the Dramatically Improved Oxygen Reduction Reaction of Jagged Platinum Nanowires, 50 Times Better than Pt. *J. Am. Chem. Soc.* **2020**, *142*, 8625–8632. [CrossRef]
89. Lin, G.; Ju, Q.; Jin, Y.; Qi, X.; Liu, W.; Huang, F.; Wang, J. Suppressing Dissolution of Pt-Based Electrocatalysts Through the Electronic Metal-Support Interaction. *Adv. Energy Mater.* **2021**, *11*, 2101050. [CrossRef]
90. Bu, L.; Ning, F.; Zhou, J.; Zhan, C.; Sun, M.; Li, L.; Zhu, Y.; Hu, Z.; Shao, Q.; Zhou, X.; et al. Three-Dimensional Porous Platinum-Tellurium-Rhodium Surface/Interface Achieve Remarkable Practical Fuel Cell Catalysis. *Energy Environ. Sci.* **2022**, *15*, 3877–3890. [CrossRef]
91. Liu, J.; Liu, S.; Yan, F.; Wen, Z.; Chen, W.; Liu, X.; Liu, Q.; Shang, J.; Yu, R.; Su, D.; et al. Ultrathin Nanotube Structure for Mass-Efficient and Durable Oxygen Reduction Reaction Catalysts in PEM Fuel Cells. *J. Am. Chem. Soc.* **2022**, *144*, 19106–19114. [CrossRef] [PubMed]
92. Song, T.-W.; Xu, C.; Sheng, Z.-T.; Yan, H.-K.; Tong, L.; Liu, J.; Zeng, W.-J.; Zuo, L.-J.; Yin, P.; Zuo, M.; et al. Small Molecule-Assisted Synthesis of Carbon Supported Platinum Intermetallic Fuel Cell Catalysts. *Nat. Commun.* **2022**, *13*, 6521. [CrossRef]
93. Göhl, D.; Garg, A.; Paciok, P.; Mayrhofer, K.J.J.; Heggen, M.; Shao-Horn, Y.; Dunin-Borkowski, R.E.; Román-Leshkov, Y.; Ledendecker, M. Engineering Stable Electrocatalysts by Synergistic Stabilization between Carbide Cores and Pt Shells. *Nat. Mater.* **2020**, *19*, 287–291. [CrossRef] [PubMed]
94. Zhuang, Y.; Yang, J.; Meng, L.; Ma, C.; Peng, L.; Chen, D.; Chen, Q. Polyaniline-Derived Carbon Nanofibers with a High Graphitization Degree Loading Ordered PtNi Intermetallic Nanoparticles for Oxygen Reduction Reaction. *Ind. Chem. Mater.* **2023**, *1*, 458–464. [CrossRef]

95. Zhao, Z.; Liu, Z.; Zhang, A.; Yan, X.; Xue, W.; Peng, B.; Xin, H.L.; Pan, X.; Duan, X.; Huang, Y. Graphene-Nanopocket-Encaged PtCo Nanocatalysts for Highly Durable Fuel Cell Operation under Demanding Ultralow-Pt-Loading Conditions. *Nat. Nanotech.* **2022**, *17*, 968–975. [CrossRef] [PubMed]
96. Huang, L.; Zaman, S.; Tian, X.; Wang, Z.; Fang, W.; Xia, B.Y. Advanced Platinum-Based Oxygen Reduction Electrocatalysts for Fuel Cells. *Acc. Chem. Res.* **2021**, *54*, 311–322. [CrossRef]
97. Yin, P.; Yan, Q.Q.; Liang, H.W. Strong Metal-Support Interactions through Sulfur-Anchoring of Metal Catalysts on Carbon Supports. *Angew. Chem. Int. Ed.* **2023**, *62*, e202302819. [CrossRef]
98. Qiao, Z.; Hwang, S.; Li, X.; Wang, C.; Samarakoon, W.; Karakalos, S.; Li, D.; Chen, M.; He, Y.; Wang, M.; et al. 3D Porous Graphitic Nanocarbon for Enhancing the Performance and Durability of Pt Catalysts: A Balance between Graphitization and Hierarchical Porosity. *Energy Environ. Sci.* **2019**, *12*, 2830–2841. [CrossRef]
99. Huang, L.; Wei, M.; Qi, R.; Dong, C.-L.; Dang, D.; Yang, C.-C.; Xia, C.; Chen, C.; Zaman, S.; Li, F.-M.; et al. An Integrated Platinum-Nanocarbon Electrocatalyst for Efficient Oxygen Reduction. *Nat. Commun.* **2022**, *13*, 6703. [CrossRef]
100. Zeng, L.; Zhao, Z.; Huang, Q.; Zhou, C.; Chen, W.; Wang, K.; Li, M.; Lin, F.; Luo, H.; Gu, Y.; et al. Single-Atom Cr-N_4 Sites with High Oxophilicity Interfaced with Pt Atomic Clusters for Practical Alkaline Hydrogen Evolution Catalysis. *J. Am. Chem. Soc.* **2023**, *145*, 21432–21441. [CrossRef]
101. Lai, J.; Chen, S.; Liu, X.; Yan, X.; Qin, Z.; Xie, L.; Lin, Z.; Cai, Z.; Zhao, Y.; Wang, H.-L.; et al. Synergy between Intermetallic Pt Alloy and Porous Co-N_4 Carbon Nanofibers Enables Durable Fuel Cells with Low Mass Transport Resistance. *ACS Catal.* **2023**, *13*, 11996–12006. [CrossRef]
102. Xiao, F.; Wang, Y.; Xu, G.-L.; Yang, F.; Zhu, S.; Sun, C.-J.; Cui, Y.; Xu, Z.; Zhao, Q.; Jang, J.; et al. Fe-N-C Boosts the Stability of Supported Platinum Nanoparticles for Fuel Cells. *J. Am. Chem. Soc.* **2022**, *144*, 20372–20384. [CrossRef] [PubMed]
103. Huang, S.-Y.; Ganesan, P.; Park, S.; Popov, B.N. Development of a Titanium Dioxide-Supported Platinum Catalyst with Ultrahigh Stability for Polymer Electrolyte Membrane Fuel Cell Applications. *J. Am. Chem. Soc.* **2009**, *131*, 13898–13899. [CrossRef] [PubMed]
104. Zhao, L.; Zhu, J.; Zheng, Y.; Xiao, M.; Gao, R.; Zhang, Z.; Wen, G.; Dou, H.; Deng, Y.-P.; Yu, A.; et al. Materials Engineering toward Durable Electrocatalysts for Proton Exchange Membrane Fuel Cells. *Adv. Energy Mater.* **2022**, *12*, 2102665. [CrossRef]
105. Zhang, Y.; Zhang, X.; Cheng, C.; Yang, Z. Recent Progress of MXenes as the Support of Catalysts for the CO Oxidation and Oxygen Reduction Reaction. *Chin. Chem. Lett.* **2020**, *31*, 931–936. [CrossRef]
106. Xu, C.; Fan, C.; Zhang, X.; Chen, H.; Liu, X.; Fu, Z.; Wang, R.; Hong, T.; Cheng, J. MXene ($Ti_3C_2T_x$) and Carbon Nanotube Hybrid-Supported Platinum Catalysts for the High-Performance Oxygen Reduction Reaction in PEMFC. *ACS Appl. Mater. Interfaces* **2020**, *12*, 19539–19546. [CrossRef] [PubMed]
107. Li, X.; Huang, Y.; Chen, Z.; Hu, S.; Zhu, J.; Tsiakaras, P.; Kang Shen, P. Novel PtNi Nanoflowers Regulated by a Third Element (Rh, Ru, Pd) as Efficient Multifunctional Electrocatalysts for ORR, MOR and HER. *Chem. Eng. J.* **2023**, *454*, 140131. [CrossRef]
108. Liu, H.; Jia, R.; Qin, C.; Yang, Q.; Tang, Z.; Li, M.; Ma, Z. Anti-CO Poisoning FePtRh Nanoflowers with Rh-Rich Core and Fe-Rich Shell Boost Methanol Oxidation Electrocatalysis. *Adv. Funct. Mater.* **2023**, *33*, 2210626. [CrossRef]
109. Duan, X.; Cao, F.; Ding, R.; Li, X.; Li, Q.; Aisha, R.; Zhang, S.; Hua, K.; Rui, Z.; Wu, Y.; et al. Cobalt-Doping Stabilized Active and Durable Sub-2 nm Pt Nanoclusters for Low-Pt-Loading PEMFC Cathode. *Adv. Energy Mater.* **2022**, *12*, 2103144. [CrossRef]
110. Li, M.; Zhao, Z.; Zhang, W.; Luo, M.; Tao, L.; Sun, Y.; Xia, Z.; Chao, Y.; Yin, K.; Zhang, Q.; et al. Sub-Monolayer YO_x/MoO_x on Ultrathin Pt Nanowires Boosts Alcohol Oxidation Electrocatalysis. *Adv. Mater.* **2021**, *33*, 2103762. [CrossRef]
111. Jin, C.; Wang, Q.; Liu, J. Pb Induced Dislocation Defects of PtCo Systems: Strain-Triggered Oxygen Reduction Reaction for PEMFC. *Nano Res.* **2023**. [CrossRef]
112. Huang, Y.; Li, M.; Yang, W.; Yu, Y.; Hao, S. Ce-Doped Ordered Mesoporous Cobalt Ferrite Phosphides as Robust Catalysts for Water Oxidation. *Chem. Eur. J.* **2020**, *26*, 13305–13310. [CrossRef] [PubMed]
113. Guo, X.; Li, M.; He, L.; Geng, S.; Tian, F.; Song, Y.; Yang, W.; Yu, Y. Industrially Promising NiCoP Nanorod Arrays Tailored with Trace W and Mo Atoms for Boosting Large-Current-Density Overall Water Splitting. *Nanoscale* **2021**, *13*, 14179–14185. [CrossRef]
114. Li, M.; Zhao, Z.; Xia, Z.; Yang, Y.; Luo, M.; Huang, Y.; Sun, Y.; Chao, Y.; Yang, W.; Yang, W.; et al. Lavender-Like Ga-Doped Pt_3Co Nanowires for Highly Stable and Active Electrocatalysis. *ACS Catal.* **2020**, *10*, 3018–3026. [CrossRef]
115. Zhang, S.; Saji, S.E.; Yin, Z.; Zhang, H.; Du, Y.; Yan, C.-H. Rare-Earth Incorporated Alloy Catalysts: Synthesis, Properties, and Applications. *Adv. Mater.* **2021**, *33*, 2005988. [CrossRef]
116. Wang, C.-Y.; Chen, L.-F.; Li, G.; Lu, B.-A.; Zhou, Z.-Y.; Tian, N.; Sun, S.-G. Improved Stability of Octahedral PtCu by Rh Doping for the Oxygen Reduction Reaction. *ChemElectroChem* **2021**, *8*, 2425–2430. [CrossRef]
117. Huang, X.; Zhao, Z.; Cao, L.; Chen, Y.; Zhu, E.; Lin, Z.; Li, M.; Yan, A.; Zettl, A.; Wang, Y.M.; et al. High-Performance Transition Metal-Doped Pt_3Ni Octahedra for Oxygen Reduction Reaction. *Science* **2015**, *348*, 1230–1234. [CrossRef]
118. Huang, H.; Li, K.; Chen, Z.; Luo, L.; Gu, Y.; Zhang, D.; Ma, C.; Si, R.; Yang, J.; Peng, Z.; et al. Achieving Remarkable Activity and Durability toward Oxygen Reduction Reaction Based on Ultrathin Rh-Doped Pt Nanowires. *J. Am. Chem. Soc.* **2017**, *139*, 8152–8159. [CrossRef]
119. Beermann, V.; Gocyla, M.; Willinger, E.; Rudi, S.; Heggen, M.; Dunin-Borkowski, R.E.; Willinger, M.-G.; Strasser, P. Rh-Doped Pt-Ni Octahedral Nanoparticles: Understanding the Correlation Between Elemental Distribution, Oxygen Reduction Reaction, and Shape Stability. *Nano Lett.* **2016**, *16*, 1719–1725. [CrossRef]

120. Lim, J.; Shin, H.; Kim, M.; Lee, H.; Lee, K.-S.; Kwon, Y.; Song, D.; Oh, S.; Kim, H.; Cho, E. Ga-Doped Pt-Ni Octahedral Nanoparticles as a Highly Active and Durable Electrocatalyst for Oxygen Reduction Reaction. *Nano Lett.* **2018**, *18*, 2450–2458. [CrossRef]
121. Tu, W.; Chen, K.; Zhu, L.; Zai, H.; Bin, E.; Ke, X.; Chen, C.; Sui, M.; Chen, Q.; Li, Y. Tungsten-Doping-Induced Surface Reconstruction of Porous Ternary Pt-Based Alloy Electrocatalyst for Oxygen Reduction. *Adv. Funct. Mater.* **2019**, *29*, 1807070. [CrossRef]
122. Wang, H.; Gao, J.; Chen, C.; Zhao, W.; Zhang, Z.; Li, D.; Chen, Y.; Wang, C.; Zhu, C.; Ke, X.; et al. PtNi-W/C with Atomically Dispersed Tungsten Sites Toward Boosted ORR in Proton Exchange Membrane Fuel Cell Devices. *Nano-Micro Lett.* **2023**, *15*, 143. [CrossRef] [PubMed]
123. Tu, W.; Luo, W.; Chen, C.; Chen, K.; Zhu, E.; Zhao, Z.; Wang, Z.; Hu, T.; Zai, H.; Ke, X.; et al. Tungsten as "Adhesive" in $Pt_2CuW_{0.25}$ Ternary Alloy for Highly Durable Oxygen Reduction Electrocatalysis. *Adv. Funct. Mater.* **2020**, *30*, 1908230. [CrossRef]
124. Zhu, S.; Sun, M.; Mei, B.; Yang, L.; Chu, Y.; Shi, Z.; Bai, J.; Wang, X.; Jiang, Z.; Liu, C.; et al. Intrinsic Spin Shielding Effect in Platinum-Rare-Earth Alloy Boosts Oxygen Reduction Activity. *Natl. Sci. Rev.* **2023**, *10*, nwad162. [CrossRef]
125. Liu, Y.; Sheng, S.; Wu, M.; Wang, S.; Wang, Y.; Yang, H.; Chen, J.; Hao, X.; Zhi, C.; Wang, Y.; et al. Controllable Synthesis of PtIrCu Ternary Alloy Ultrathin Nanowires for Enhanced Ethanol Electrooxidation. *ACS Appl. Mater. Interfaces* **2023**, *15*, 3934–3940. [CrossRef]
126. Cao, J.; Cao, H.; Wang, F.; Zhu, H. Zigzag PtCo Nanowires Modified in situ with Au Atoms as Efficient and Durable Electrocatalyst for Oxygen Reduction Reaction. *J. Power Sources* **2021**, *489*, 229425. [CrossRef]
127. Greeley, J.; Stephens, I.E.L.; Bondarenko, A.S.; Johansson, T.P.; Hansen, H.A.; Jaramillo, T.F.; Rossmeisl, J.; Chorkendorff, I.; Nørskov, J.K. Alloys of Platinum and Early Transition Metals as Oxygen Reduction Electrocatalysts. *Nat. Chem.* **2009**, *1*, 552–556. [CrossRef]
128. Gao, L.; Sun, T.; Tan, X.; Liu, M.; Xue, F.; Wang, B.; Zhang, J.; Lu, Y.-F.; Ma, C.; Tian, H.; et al. Trace Doping of Early Transition Metal Enabled Efficient and Durable Oxygen Reduction Catalysis on Pt-Based Ultrathin Nanowires. *Appl. Catal. B* **2022**, *303*, 120918. [CrossRef]
129. Chao, T.; Luo, X.; Zhu, M.; Hu, Y.; Zhang, Y.; Qu, Y.; Peng, H.; Shen, X.; Zheng, X.; Zhang, L.; et al. The Promoting Effect of Interstitial Hydrogen on the Oxygen Reduction Performance of PtPd Alloy Nanotubes for Fuel Cells. *Nano Res.* **2023**, *16*, 2366–2372. [CrossRef]
130. Li, Z.; Niu, W.; Yang, Z.; Zaman, N.; Samarakoon, W.; Wang, M.; Kara, A.; Lucero, M.; Vyas, M.V.; Cao, H.; et al. Stabilizing Atomic Pt with Trapped Interstitial F in Alloyed PtCo Nanosheets for High-Performance Zinc-Air Batteries. *Energy Environ. Sci.* **2020**, *13*, 884–895. [CrossRef]
131. Mao, Z.; Ding, C.; Liu, X.; Zhang, Q.; Qin, X.; Li, H.; Yang, F.; Li, Q.; Zhang, X.-G.; Zhang, J.; et al. Interstitial B-Doping in Pt Lattice to Upgrade Oxygen Electroreduction Performance. *ACS Catal.* **2022**, *12*, 8848–8856. [CrossRef]
132. Shi, F.; Peng, J.; Li, F.; Qian, N.; Shan, H.; Tao, P.; Song, C.; Shang, W.; Deng, T.; Zhang, H.; et al. Design of Highly Durable Core-Shell Catalysts by Controlling Shell Distribution Guided by in-situ Corrosion Study. *Adv. Mater.* **2021**, *33*, 2101511. [CrossRef] [PubMed]
133. Zhao, X.; Sasaki, K. Advanced Pt-Based Core-Shell Electrocatalysts for Fuel Cell Cathodes. *Acc. Chem. Res.* **2022**, *55*, 1226–1236. [CrossRef] [PubMed]
134. Gong, S.; Zhang, Y.-X.; Niu, Z. Recent Advances in Earth-Abundant Core/Noble-Metal Shell Nanoparticles for Electrocatalysis. *ACS Catal.* **2020**, *10*, 10886–10904. [CrossRef]
135. Li, M.; Zhao, Z.; Xia, Z.; Luo, M.; Zhang, Q.; Qin, Y.; Tao, L.; Yin, K.; Chao, Y.; Gu, L.; et al. Exclusive Strain Effect Boosts Overall Water Splitting in PdCu/Ir Core/Shell Nanocrystals. *Angew. Chem. Int. Ed.* **2021**, *60*, 8243–8250. [CrossRef] [PubMed]
136. Wu, Z.-P.; Shan, S.; Zang, S.-Q.; Zhong, C.-J. Dynamic Core-Shell and Alloy Structures of Multimetallic Nanomaterials and Their Catalytic Synergies. *Acc. Chem. Res.* **2020**, *53*, 2913–2924. [CrossRef] [PubMed]
137. Sasaki, K.; Kuttiyiel, K.A.; Adzic, R.R. Designing High Performance Pt Monolayer Core-Shell Electrocatalysts for Fuel Cells. *Curr. Opin. Electrochem.* **2020**, *21*, 368–375. [CrossRef]
138. Sasaki, K.; Naohara, H.; Choi, Y.; Cai, Y.; Chen, W.-F.; Liu, P.; Adzic, R.R. Highly Stable Pt Monolayer on PdAu Nanoparticle Electrocatalysts for the Oxygen Reduction Reaction. *Nat. Commun.* **2012**, *3*, 1115. [CrossRef]
139. Zhao, F.; Zheng, L.; Yuan, Q.; Zhang, Q.; Sheng, T.; Yang, X.; Gu, L.; Wang, X. PtCu Subnanoclusters Epitaxial on Octahedral PtCu/Pt Skin Matrix as Ultrahigh Stable Cathode Electrocatalysts for Room-Temperature Hydrogen Fuel Cells. *Nano Res.* **2023**, *16*, 2252–2258. [CrossRef]
140. Wang, Z.; Chen, S.; Wu, W.; Chen, R.; Zhu, Y.; Jiang, H.; Yu, L.; Cheng, N. Tailored Lattice Compressive Strain of Pt-Skins by the $L1_2$-Pt_3M Intermetallic Core for Highly Efficient Oxygen Reduction. *Adv. Mater.* **2023**, *35*, 2301310. [CrossRef]
141. Wang, G.; Huang, B.; Xiao, L.; Ren, Z.; Chen, H.; Wang, D.; Abruña, H.D.; Lu, J.; Zhuang, L. Pt Skin on AuCu Intermetallic Substrate: A Strategy to Maximize Pt Utilization for Fuel Cells. *J. Am. Chem. Soc.* **2014**, *136*, 9643–9649. [CrossRef] [PubMed]
142. Luo, M.; Sun, Y.; Zhang, X.; Qin, Y.; Li, M.; Li, Y.; Li, C.; Yang, Y.; Wang, L.; Gao, P.; et al. Stable High-Index Faceted Pt Skin on Zigzag-Like PtFe Nanowires Enhances Oxygen Reduction Catalysis. *Adv. Mater.* **2018**, *30*, 1705515. [CrossRef] [PubMed]
143. Zhang, Y.; Lyu, Z.; Chen, Z.; Zhu, S.; Shi, Y.; Chen, R.; Xie, M.; Yao, Y.; Chi, M.; Shao, M.; et al. Maximizing the Catalytic Performance of $Pd@Au_xPd_{1-x}$ Nanocubes in H_2O_2 Production by Reducing Shell Thickness to Increase Compositional Stability. *Angew. Chem. Int. Ed.* **2021**, *60*, 19643–19647. [CrossRef] [PubMed]

144. Kuttiyiel, K.A.; Sasaki, K.; Choi, Y.; Su, D.; Liu, P.; Adzic, R.R. Nitride Stabilized PtNi Core-Shell Nanocatalyst for High Oxygen Reduction Activity. *Nano Lett.* **2012**, *12*, 6266–6271. [CrossRef] [PubMed]
145. Lee, E.; Kuttiyiel, K.A.; Kim, K.-H.; Jang, J.; Lee, H.J.; Lee, J.M.; Seo, M.H.; Yang, T.-H.; Yim, S.-D.; Vargas, J.A.; et al. High Pressure Nitrogen-Infused Ultrastable Fuel Cell Catalyst for Oxygen Reduction Reaction. *ACS Catal.* **2021**, *11*, 5525–5531. [CrossRef]
146. Guo, H.; Li, L.; Chen, Y.; Zhang, W.; Shang, C.; Cao, X.; Li, M.; Zhang, Q.; Tan, H.; Nie, Y.; et al. Precise Strain Tuning Boosts Electrocatalytic Hydrogen Generation. *Adv. Mater.* **2023**, *35*, 2302285. [CrossRef] [PubMed]
147. Kluge, R.M.; Haid, R.W.; Riss, A.; Bao, Y.; Seufert, K.; Schmidt, T.O.; Watzele, S.A.; Barth, J.V.; Allegretti, F.; Auwärter, W.; et al. A Trade-Off Between Ligand and Strain Effects Optimizes the Oxygen Reduction Activity of Pt Alloys. *Energy Environ. Sci.* **2022**, *15*, 5181–5191. [CrossRef]
148. Li, M.; Luo, M.; Xia, Z.; Yang, Y.; Huang, Y.; Wu, D.; Sun, Y.; Li, C.; Chao, Y.; Yang, W.; et al. Modulating the Surface Segregation of PdCuRu Nanocrystals for Enhanced All-pH Hydrogen Evolution Electrocatalysis. *J. Mater. Chem. A* **2019**, *7*, 20151–20157. [CrossRef]
149. Adit Maark, T.; Peterson, A.A. Understanding Strain and Ligand Effects in Hydrogen Evolution over Pd(111) Surfaces. *J. Phy. Chem. C* **2014**, *118*, 4275–4281. [CrossRef]
150. Liu, M.; Xin, H.; Wu, Q. Unusual Strain Effect of a Pt-Based $L1_0$ Face-Centered Tetragonal Core in Core/Shell Nanoparticles for the Oxygen Reduction Reaction. *Phys. Chem. Chem. Phys.* **2019**, *21*, 6477–6484. [CrossRef]
151. Guo, L.-M.; Zhang, D.-F.; Guo, L. Structure Design Reveals the Role of Au for ORR Catalytic Performance Optimization in PtCo-Based Catalysts. *Adv. Funct. Mater.* **2020**, *30*, 2001575. [CrossRef]
152. Luo, M.; Yang, Y.; Sun, Y.; Qin, Y.; Li, C.; Li, Y.; Li, M.; Zhang, S.; Su, D.; Guo, S. Ultrathin Two-Dimensional Metallic Nanocrystals for Renewable Energy Electrocatalysis. *Mater. Today* **2019**, *23*, 45–56. [CrossRef]
153. Kang, Y.; Wang, J.; Wei, Y.; Wu, Y.; Xia, D.; Gan, L. Engineering Nanoporous and Solid Core-Shell Architectures of Low-Platinum Alloy Catalysts for High Power Density PEM Fuel Cells. *Nano Res.* **2022**, *15*, 6148–6155. [CrossRef]
154. Tao, L.; Huang, B.; Jin, F.; Yang, Y.; Luo, M.; Sun, M.; Liu, Q.; Gao, F.; Guo, S. Atomic PdAu Interlayer Sandwiched into Pd/Pt Core/Shell Nanowires Achieves Superstable Oxygen Reduction Catalysis. *ACS Nano* **2020**, *14*, 11570–11578. [CrossRef] [PubMed]
155. Huang, L.; Zheng, C.Y.; Shen, B.; Mirkin, C.A. High-Index-Facet Metal-Alloy Nanoparticles as Fuel Cell Electrocatalysts. *Adv. Mater.* **2020**, *32*, 2002849. [CrossRef] [PubMed]
156. Luo, M.; Sun, Y.; Qin, Y.; Chen, S.; Li, Y.; Li, C.; Yang, Y.; Wu, D.; Xu, N.; Xing, Y.; et al. Surface and Near-Surface Engineering of PtCo Nanowires at Atomic Scale for Enhanced Electrochemical Sensing and Catalysis. *Chem. Mater.* **2018**, *30*, 6660–6667. [CrossRef]
157. Jin, H.; Xu, Z.; Hu, Z.-Y.; Yin, Z.; Wang, Z.; Deng, Z.; Wei, P.; Feng, S.; Dong, S.; Liu, J.; et al. Mesoporous Pt@Pt-Skin Pt_3Ni Core-Shell Framework Nanowire Electrocatalyst for Efficient Oxygen Reduction. *Nat. Commun.* **2023**, *14*, 1518. [CrossRef]
158. Bu, L.; Zhang, N.; Guo, S.; Zhang, X.; Li, J.; Yao, J.; Wu, T.; Lu, G.; Ma, J.-Y.; Su, D.; et al. Biaxially Strained PtPb/Pt Core/Shell Nanoplate Boosts Oxygen Reduction Catalysis. *Science* **2016**, *354*, 1410–1414. [CrossRef]
159. Gao, P.; Pu, M.; Chen, Q.; Zhu, H. Pt-Based Intermetallic Nanocrystals in Cathode Catalysts for Proton Exchange Membrane Fuel Cells: From Precise Synthesis to Oxygen Reduction Reaction Strategy. *Catalysts* **2021**, *11*, 1050. [CrossRef]
160. Li, J.; Sun, S. Intermetallic Nanoparticles: Synthetic Control and Their Enhanced Electrocatalysis. *Acc. Chem. Res.* **2019**, *52*, 2015–2025. [CrossRef]
161. Lin, F.; Li, M.; Zeng, L.; Luo, M.; Guo, S. Intermetallic Nanocrystals for Fuel-Cells-Based Electrocatalysis. *Chem. Rev.* **2023**, *123*, 12507–12593. [CrossRef] [PubMed]
162. Zhou, M.; Li, C.; Fang, J. Noble-Metal Based Random Alloy and Intermetallic Nanocrystals: Syntheses and Applications. *Chem. Rev.* **2021**, *121*, 736–795. [CrossRef]
163. Xiao, W.; Lei, W.; Gong, M.; Xin, H.L.; Wang, D. Recent Advances of Structurally Ordered Intermetallic Nanoparticles for Electrocatalysis. *ACS Catal.* **2018**, *8*, 3237–3256. [CrossRef]
164. Li, M.; Xia, Z.; Huang, Y.; Tao, L.; Chao, Y.; Yin, K.; Yang, W.; Yang, W.; Yu, Y.; Guo, S. Rh-Doped PdCu Ordered Intermetallics for Enhanced Oxygen Reduction Electrocatalysis with Superior Methanol Tolerance. *Acta Phys.-Chin. Sin.* **2020**, *36*, 1912049.
165. Liao, Y.; Peng, L.; Wu, C.; Yan, Y.; Xie, H.; Chen, Y.; Wang, Y. Size and Near-Surface Engineering in Weak-Oxidative Confined Space to Fabricate 4 nm $L1_0$-PtCo@Pt Nanoparticles for Oxygen Reduction Reaction. *Nano Res.* **2023**, *16*, 6622–6631. [CrossRef]
166. Feng, G.; Ning, F.; Pan, Y.; Chen, T.; Song, J.; Wang, Y.; Zou, R.; Su, D.; Xia, D. Engineering Structurally Ordered High-Entropy Intermetallic Nanoparticles with High-Activity Facets for Oxygen Reduction in Practical Fuel Cells. *J. Am. Chem. Soc.* **2023**, *145*, 11140–11150. [CrossRef] [PubMed]
167. Li, J.; Xi, Z.; Pan, Y.-T.; Spendelow, J.S.; Duchesne, P.N.; Su, D.; Li, Q.; Yu, C.; Yin, Z.; Shen, B.; et al. Fe Stabilization by Intermetallic $L1_0$-FePt and Pt Catalysis Enhancement in $L1_0$-FePt/Pt Nanoparticles for Efficient Oxygen Reduction Reaction in Fuel Cells. *J. Am. Chem. Soc.* **2018**, *140*, 2926–2932. [CrossRef]
168. Li, J.; Sharma, S.; Liu, X.; Pan, Y.-T.; Spendelow, J.S.; Chi, M.; Jia, Y.; Zhang, P.; Cullen, D.A.; Xi, Z.; et al. Hard-Magnet $L1_0$-CoPt Nanoparticles Advance Fuel Cell Catalysis. *Joule* **2019**, *3*, 124–135. [CrossRef]
169. Liu, X.; Zhao, Z.; Liang, J.; Li, S.; Lu, G.; Priest, C.; Wang, T.; Han, J.; Wu, G.; Wang, X.; et al. Inducing Covalent Atomic Interaction in Intermetallic Pt Alloy Nanocatalysts for High-Performance Fuel Cells. *Angew. Chem. Int. Ed.* **2023**, *62*, e202302134. [CrossRef]
170. Kim, J.; Rong, C.; Liu, J.P.; Sun, S. Dispersible Ferromagnetic FePt Nanoparticles. *Adv. Mater.* **2009**, *21*, 906–909. [CrossRef]

171. Wang, T.; Liang, J.; Zhao, Z.; Li, S.; Lu, G.; Xia, Z.; Wang, C.; Luo, J.; Han, J.; Ma, C.; et al. Sub-6 nm Fully Ordered $L1_0$-Pt-Ni-Co Nanoparticles Enhance Oxygen Reduction via Co Doping Induced Ferromagnetism Enhancement and Optimized Surface Strain. *Adv. Energy Mater.* **2019**, *9*, 1803771. [CrossRef]
172. Cui, Z.; Chen, H.; Zhao, M.; Marshall, D.; Yu, Y.; Abruña, H.; DiSalvo, F.J. Synthesis of Structurally Ordered Pt_3Ti and Pt_3V Nanoparticles as Methanol Oxidation Catalysts. *J. Am. Chem. Soc.* **2014**, *136*, 10206–10209. [CrossRef] [PubMed]
173. Zhao, W.; Ye, Y.; Jiang, W.; Li, J.; Tang, H.; Hu, J.; Du, L.; Cui, Z.; Liao, S. Mesoporous Carbon Confined Intermetallic Nanoparticles as Highly Durable Electrocatalysts for the Oxygen Reduction Reaction. *J. Mater. Chem. A* **2020**, *8*, 15822–15828. [CrossRef]
174. Gong, Q.; Zhang, H.; Yu, H.; Jeon, S.; Ren, Y.; Yang, Z.; Sun, C.-J.; Stach, E.A.; Foucher, A.C.; Yu, Y.; et al. Amino-Tethering Synthesis Strategy Toward Highly Accessible Sub-3-nm $L1_0$-PtM Catalysts for High-Power Fuel Cells. *Matter* **2023**, *6*, 963–982. [CrossRef]
175. Cheng, H.; Gui, R.; Yu, H.; Wang, C.; Liu, S.; Liu, H.; Zhou, T.; Zhang, N.; Zheng, X.; Chu, W.; et al. Subsize Pt-based Intermetallic Compound Enables Long-Term Cyclic Mass Activity for Fuel-Cell Oxygen Reduction. *Proc. Natl. Acad. Sci. USA* **2021**, *118*, e2104026118. [CrossRef]
176. Liang, J.; Zhao, Z.; Li, N.; Wang, X.; Li, S.; Liu, X.; Wang, T.; Lu, G.; Wang, D.; Hwang, B.-J.; et al. Biaxial Strains Mediated Oxygen Reduction Electrocatalysis on Fenton Reaction Resistant $L1_0$-PtZn Fuel Cell Cathode. *Adv. Energy Mater.* **2020**, *10*, 2000179. [CrossRef]
177. Yang, C.-L.; Wang, L.-N.; Yin, P.; Liu, J.; Chen, M.-X.; Yan, Q.-Q.; Wang, Z.-S.; Xu, S.-L.; Chu, S.-Q.; Cui, C.; et al. Sulfur-Anchoring Synthesis of Platinum Intermetallic Nanoparticle Catalysts for Fuel Cells. *Science* **2021**, *374*, 459–464. [CrossRef]
178. Li, J.; Sharma, S.; Wei, K.; Chen, Z.; Morris, D.; Lin, H.; Zeng, C.; Chi, M.; Yin, Z.; Muzzio, M.; et al. Anisotropic Strain Tuning of $L1_0$ Ternary Nanoparticles for Oxygen Reduction. *J. Am. Chem. Soc.* **2020**, *142*, 19209–19216. [CrossRef]
179. Yang, Z.; Yang, H.; Shang, L.; Zhang, T. Ordered PtFeIr Intermetallic Nanowires Prepared through a Silica-Protection Strategy for the Oxygen Reduction Reaction. *Angew. Chem. Int. Ed.* **2022**, *61*, e202113278. [CrossRef]
180. Kim, H.Y.; Kim, J.M.; Ha, Y.; Woo, J.; Byun, A.; Shin, T.J.; Park, K.H.; Jeong, H.Y.; Kim, H.; Kim, J.Y.; et al. Activity Origin and Multifunctionality of Pt-Based Intermetallic Nanostructures for Efficient Electrocatalysis. *ACS Catal.* **2019**, *9*, 11242–11254. [CrossRef]
181. Kim, H.Y.; Kwon, T.; Ha, Y.; Jun, M.; Baik, H.; Jeong, H.Y.; Kim, H.; Lee, K.; Joo, S.H. Intermetallic PtCu Nanoframes as Efficient Oxygen Reduction Electrocatalysts. *Nano Lett.* **2020**, *20*, 7413–7421. [CrossRef] [PubMed]
182. Qin, Y.; Luo, M.; Sun, Y.; Li, C.; Huang, B.; Yang, Y.; Li, Y.; Wang, L.; Guo, S. Intermetallic *hcp*-PtBi/*fcc*-Pt Core/Shell Nanoplates Enable Efficient Bifunctional Oxygen Reduction and Methanol Oxidation Electrocatalysis. *ACS Catal.* **2018**, *8*, 5581–5590. [CrossRef]
183. Lv, H.; Wang, Y.; Sun, L.; Yamauchi, Y.; Liu, B. A General Protocol for Precise Syntheses of Ordered Mesoporous Intermetallic Nanoparticles. *Nat. Protoc.* **2023**, *18*, 3126–3154. [CrossRef]
184. Lv, H.; Zheng, Y.; Wang, Y.; Wang, J.; Liu, B.; Qiao, Z.-A. Ordered Mesoporous Intermetallic Ga-Pt Nanoparticles: Phase-Controlled Synthesis and Performance in Oxygen Reduction Electrocatalysis. *Angew. Chem. Int. Ed.* **2023**, *62*, e202304420. [CrossRef] [PubMed]
185. Song, T.-W.; Chen, M.-X.; Yin, P.; Tong, L.; Zuo, M.; Chu, S.-Q.; Chen, P.; Liang, H.-W. Intermetallic PtFe Electrocatalysts for the Oxygen Reduction Reaction: Ordering Degree-Dependent Performance. *Small* **2022**, *18*, 2202916. [CrossRef]
186. Chen, H.-Q.; Ze, H.; Yue, M.-F.; Wei, D.-Y.; Wu, Y.-F.; Dong, J.-C.; Zhang, Y.-J.; Zhang, H.; Tian, Z.-Q.; Li, J.-F.; et al. Unmasking the Critical Role of the Ordering Degree of Bimetallic Nanocatalysts on Oxygen Reduction Reaction by in situ Raman Spectroscopy. *Angew. Chem. Int. Ed.* **2022**, *61*, e202117834. [CrossRef]
187. Wang, Y.; Gong, N.; Liu, H.; Ma, W.; Hippalgaonkar, K.; Liu, Z.; Huang, Y. Ordering-Dependent Hydrogen Evolution and Oxygen Reduction Electrocatalysis of High-Entropy Intermetallic $Pt_4FeCoCuNi$. *Adv. Mater.* **2023**, *35*, 2302067. [CrossRef]
188. Shao, R.-Y.; Xu, X.-C.; Zhou, Z.-H.; Zeng, W.-J.; Song, T.-W.; Yin, P.; Li, A.; Ma, C.-S.; Tong, L.; Kong, Y.; et al. Promoting Ordering Degree of Intermetallic Fuel Cell Catalysts by Low-Melting-Point Metal Doping. *Nat. Commun.* **2023**, *14*, 5896. [CrossRef]
189. Guan, J.; Yang, S.; Liu, T.; Yu, Y.; Niu, J.; Zhang, Z.; Wang, F. Intermetallic FePt@PtBi Core-Shell Nanoparticles for Oxygen Reduction Electrocatalysis. *Angew. Chem. Int. Ed.* **2021**, *60*, 21899–21904. [CrossRef]
190. Chen, X.; Wang, H.; Wan, H.; Wu, T.; Shu, D.; Shen, L.; Wang, Y.; Ruterana, P.; Lund, P.D.; Wang, H. Core/Shell Cu/FePtCu Nanoparticles with Face-Centered Tetragonal Texture: An Active and Stable Low-Pt Catalyst for Enhanced Oxygen Reduction. *Nano Energy* **2018**, *54*, 280–287. [CrossRef]
191. Yao, Y.; Dong, Q.; Brozena, A.; Luo, J.; Miao, J.; Chi, M.; Wang, C.; Kevrekidis, I.G.; Ren, Z.J.; Greeley, J.; et al. High-Entropy Nanoparticles: Synthesis-Structure-Property Relationships and Data-Driven Discovery. *Science* **2022**, *376*, eabn3103. [CrossRef]
192. Han, X.; Wu, G.; Zhao, S.; Guo, J.; Yan, M.; Hong, X.; Wang, D. Nanoscale High-Entropy Alloy for Electrocatalysis. *Matter* **2023**, *6*, 1717–1751. [CrossRef]
193. Li, H.; Zhu, H.; Zhang, S.; Zhang, N.; Du, M.; Chai, Y. Nano High-Entropy Materials: Synthesis Strategies and Catalytic Applications. *Small Struct.* **2020**, *1*, 2000033. [CrossRef]
194. Wang, X.; Vasileff, A.; Jiao, Y.; Zheng, Y.; Qiao, S.-Z. Electronic and Structural Engineering of Carbon-Based Metal-Free Electrocatalysts for Water Splitting. *Adv. Mater.* **2019**, *31*, 1803625. [CrossRef] [PubMed]
195. Lu, Z.; Chen, Z.W.; Singh, C.V. Neural Network-Assisted Development of High-Entropy Alloy Catalysts: Decoupling Ligand and Coordination Effects. *Matter* **2020**, *3*, 1318–1333. [CrossRef]

196. Ma, X.; Xin, H. Orbitalwise Coordination Number for Predicting Adsorption Properties of Metal Nanocatalysts. *Phys. Rev. Lett.* **2017**, *118*, 036101. [CrossRef] [PubMed]
197. Calle-Vallejo, F.; Loffreda, D.; Koper, M.T.M.; Sautet, P. Introducing Structural Sensitivity into Adsorption-Energy Scaling Relations by Means of Coordination Numbers. *Nat. Chem.* **2015**, *7*, 403–410. [CrossRef] [PubMed]
198. Batchelor, T.A.A.; Pedersen, J.K.; Winther, S.H.; Castelli, I.E.; Jacobsen, K.W.; Rossmeisl, J. High-Entropy Alloys as a Discovery Platform for Electrocatalysis. *Joule* **2019**, *3*, 834–845. [CrossRef]
199. Pedersen, J.K.; Clausen, C.M.; Krysiak, O.A.; Xiao, B.; Batchelor, T.A.A.; Löffler, T.; Mints, V.A.; Banko, L.; Arenz, M.; Savan, A.; et al. Bayesian Optimization of High-Entropy Alloy Compositions for Electrocatalytic Oxygen Reduction. *Angew. Chem. Int. Ed.* **2021**, *60*, 24144–24152. [CrossRef]
200. Duan, J.; Wang, M.; Huang, R.; Miao, J.; Lu, Y.; Wang, T.; Li, T. A Novel High-Entropy Alloy with an Exceptional Combination of Soft Magnetic Properties and Corrosion Resistance. *Sci. China Mater.* **2023**, *66*, 772–779. [CrossRef]
201. Yu, Y.; Xia, F.; Wang, C.; Wu, J.; Fu, X.; Ma, D.; Lin, B.; Wang, J.; Yue, Q.; Kang, Y. High-Entropy Alloy Nanoparticles as a Promising Electrocatalyst to Enhance Activity and Durability for Oxygen Reduction. *Nano Res.* **2022**, *15*, 7868–7876. [CrossRef]
202. Zhang, W.; Feng, X.; Mao, Z.X.; Li, J.; Wei, Z. Stably Immobilizing Sub-3 nm High-Entropy Pt Alloy Nanocrystals in Porous Carbon as Durable Oxygen Reduction Electrocatalyst. *Adv. Funct. Mater.* **2022**, *32*, 2204110. [CrossRef]
203. Zhan, C.; Xu, Y.; Bu, L.; Zhu, H.; Feng, Y.; Yang, T.; Zhang, Y.; Yang, Z.; Huang, B.; Shao, Q.; et al. Subnanometer High-Entropy Alloy Nanowires Enable Remarkable Hydrogen Oxidation Catalysis. *Nat. Commun.* **2021**, *12*, 6261. [CrossRef] [PubMed]
204. Fu, X.; Zhang, J.; Zhan, S.; Xia, F.; Wang, C.; Ma, D.; Yue, Q.; Wu, J.; Kang, Y. High-Entropy Alloy Nanosheets for Fine-Tuning Hydrogen Evolution. *ACS Catal.* **2022**, *12*, 11955–11959. [CrossRef]
205. Jin, Z.; Lyu, J.; Zhao, Y.-L.; Li, H.; Lin, X.; Xie, G.; Liu, X.; Kai, J.-J.; Qiu, H.-J. Rugged High-Entropy Alloy Nanowires with in situ Formed Surface Spinel Oxide as Highly Stable Electrocatalyst in Zn-Air Batteries. *ACS Mater. Lett.* **2020**, *2*, 1698–1706. [CrossRef]
206. Han, G.; Li, M.; Liu, H.; Zhang, W.; He, L.; Tian, F.; Liu, Y.; Yu, Y.; Yang, W.; Guo, S. Short-Range Diffusion Enables General Synthesis of Medium-Entropy Alloy Aerogels. *Adv. Mater.* **2022**, *34*, 2202943. [CrossRef] [PubMed]
207. Tao, L.; Sun, M.; Zhou, Y.; Luo, M.; Lv, F.; Li, M.; Zhang, Q.; Gu, L.; Huang, B.; Guo, S. A General Synthetic Method for High-Entropy Alloy Subnanometer Ribbons. *J. Am. Chem. Soc.* **2022**, *144*, 10582–10590. [CrossRef]
208. Zhang, Q.; Shen, T.; Song, M.; Wang, S.; Zhang, J.; Huang, X.; Lu, S.; Wang, D. High-Entropy $L1_2$-Pt$(FeCoNiCuZn)_3$ Intermetallics for Ultrastable Oxygen Reduction Reaction. *J. Energy Chem.* **2023**, *86*, 158–166. [CrossRef]
209. Shao, Q.; Wang, P.; Huang, X. Opportunities and Challenges of Interface Engineering in Bimetallic Nanostructure for Enhanced Electrocatalysis. *Adv. Funct. Mater.* **2019**, *29*, 1806419. [CrossRef]
210. Guo, X.; Li, M.; Qiu, L.; Tian, F.; He, L.; Geng, S.; Liu, Y.; Song, Y.; Yang, W.; Yu, Y. Engineering Electron Redistribution of Bimetallic Phosphates with CeO_2 Enables High-Performance Overall Water Splitting. *Chem. Eng. J.* **2023**, *453*, 139796. [CrossRef]
211. Gbadamasi, S.; Mohiuddin, M.; Krishnamurthi, V.; Verma, R.; Khan, M.W.; Pathak, S.; Kalantar-Zadeh, K.; Mahmood, N. Interface Chemistry of Two-Dimensional Heterostructures—Fundamentals to Applications. *Chem. Soc. Rev.* **2021**, *50*, 4684–4729. [CrossRef] [PubMed]
212. Chen, J.; Qian, G.; Chu, B.; Jiang, Z.; Tan, K.; Luo, L.; Li, B.; Yin, S. Tuning *d*-Band Center of Pt by PtCo-PtSn Heterostructure for Enhanced Oxygen Reduction Reaction Performance. *Small* **2022**, *18*, 2106773. [CrossRef] [PubMed]